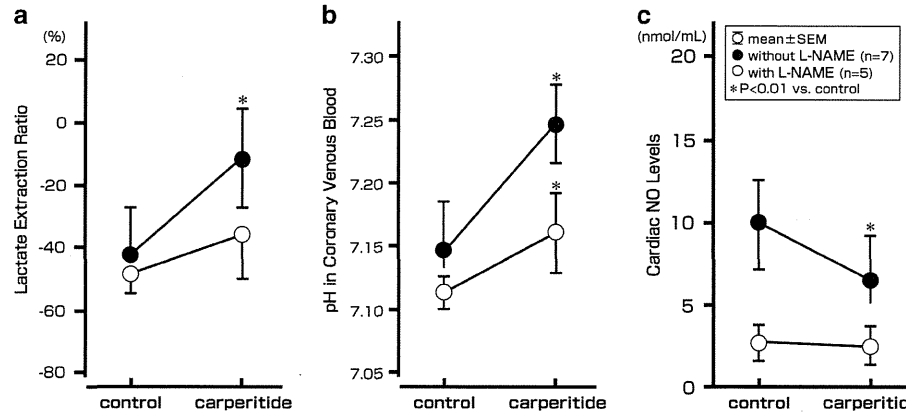

Figure 6 Effects of carperitide on metabolic function in ischemic hearts with or without L$^{\omega}$-nitroarginine methyl ester (L-NAME). Carperitide increased both (**a**) lactate extraction ratio LER and (**b**) pH levels in coronary venous blood from the ischemic area; L-NAME blunted these effects without increasing cardiac nitric oxide (NO) levels (**c**). *$P<0.01$ *vs.* the control.

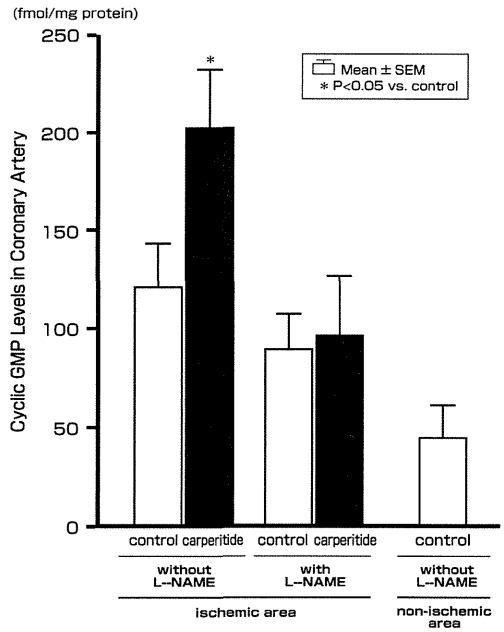

Figure 7 Cyclic guanosine monophosphate (GMP) levels in the coronary arteries of ischemic hearts. Ischemia *per se* increased cyclic GMP levels that were further elevated by carperitide. The increases in cyclic GMP levels were attenuated by Lω-nitroarginine methyl ester (L-NAME). *$P<0.05$ *vs.* the control.

with carperitide or carperitide and L-NAME, respectively; $P<0.05$; Figure 8a). Figure 8b shows the regression plots of the area at risk and endocardial collateral blood flow during ischemia. Carperitide mediated the substantial cardioprotection irrespective of collateral flow that was again blunted by L-NAME.

DISCUSSION

The present study showed that carperitide causes coronary vasodilation and promotes myocardial contractility and metabolism in ischemic hearts, the effects that are mediated by accumulation of cyclic GMP in the coronary artery and myocardium. In addition, carperitide potently decreases the infarct size following sustained ischemia and reperfusion. We also showed that inhibiting NO production attenuates carperitide-induced coronary vasodilation and reductions in the infarct size.

Table 1 Risk area and endocardial collateral blood flow during myocardial ischemia in each group

Groups	*Risk area* (%)	*Collateral blood flow during myocardial ischemia* (ml per 100g per min)
1. Control group	39.3±2.0	8.4±1.6
2. Carperitide group	40.6±1.8	7.7±1.6
3. Carperitide + L-NAME group	42.3±2.5	10.4±1.3
4. L-NAME group	39.2±1.3	7.8±1.9

Abbreviation: L-NAME, L$^{\omega}$-nitroarginine methyl ester.
Values are expressed as means±s.e.m. There were no significant differences in the area at risk or coronary blood flow (CBF) among any of the groups.

Role of NO in carperitide-mediated coronary vasodilation in ischemic hearts

The present study showed that carperitide increases CBF in a manner dependent on cyclic GMP. Because cyclic GMP induces vasorelaxation in smooth muscle cells, the carperitide-induced coronary vasodilation was likely a result of increased cyclic GMP levels. Several other effects of carperitide, however, should be considered. First of all, because carperitide attenuates catecholamine-induced cellular responses,[23] the reduction of α-adrenoceptor activation by carperitide may cause coronary vasodilation. Indeed, we could not exclude the possibility that the carperitide-induced coronary vasodilation is mediated by coronary α_2-adrenoceptor blockade. On the other hand, myocardial effects of carperitide may also be involved in the present observation. If this myocardial effect of carperitide was the case, carperitide should have also reduced norepinephrine-induced myocardial hypercontraction, leading to lower myocardial contractility and oxygen consumption. However, the present study revealed that carperitide did not alter myocardial oxygen consumption (Figure 1). It is well known that an increase in coronary perfusion increases myocardial oxygen consumption, termed the Gregg phenomenon. In turn, carperitide has a potency to decrease myocardial oxygen consumption via increased myocardial cyclic GMP levels that may blunt the Gregg phenomenon. We may have observed the mixed effects of carperitide

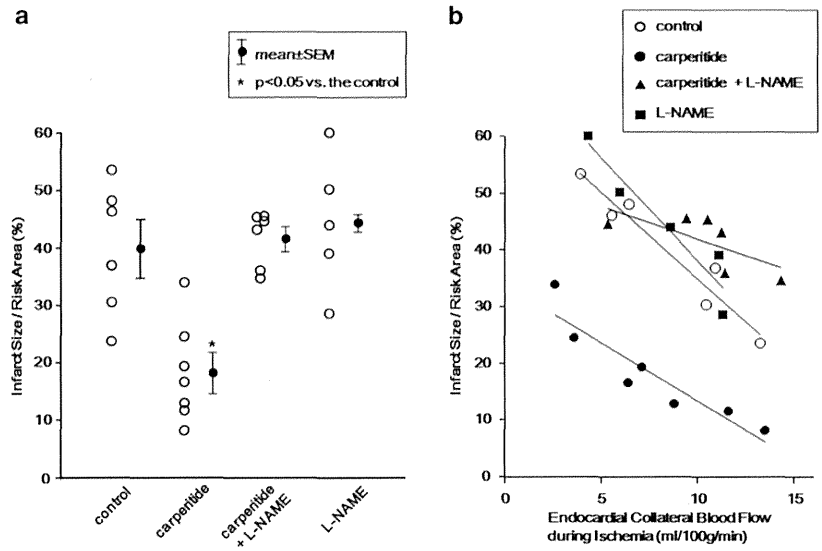

Figure 8 Effects of carperitide on myocardial ischemia and reperfusion. (**a**) Infarcts were smaller in the carperitide group compared with the control group, a difference that was abolished by L^{ω}-nitroarginine methyl ester (L-NAME). Infarct size expressed as the plot of infarct size because of 90 min of ischemia and regional collateral flow during ischemia (**b**). There are inverse relations between normalized infarct area and collateral flow, and a significant difference ($P<0.05$) is seen in the carperitide group compared with the control group. ANP, atrial natriuretic peptide. $^{*}P<0.05$ *vs.* the control group.

that may culminate in no changes in myocardial oxygen consumption. Second, because (1) NO increases CBF[24] and (2) L-NAME attenuates carperitide-induced coronary vasodilation, carperitide may enhance NO production. Because the levels of the end-product of cardiac NO (Figures 4c and 6c) did not increase in response to carperitide, this possibility appears unlikely. Third, carperitide may inhibit leukocyte activation and adhesion that occur in ischemic hearts.[25] Because leukocyte adhesion decreases CBF by plugging small coronary arteries, reduced leukocyte adhesion may restore CBF. However, this would not be likely. A significant amount of binding between leukocytes and coronary endothelial cells would be required to reduce CBF, and this degree of adhesion would not likely be attenuated quickly following carperitide infusion. The effects of carperitide, however, were reversible as shown in Figures 2 and 3. Fourth, carperitide may open collateral flow that may increase CBF. In the present study, carperitide increased CBF in the perfused region that was measured with an electromagnetic flow probe attached to the bypass tube in the coronary hypoperfusion model (Figure 2b), indicating that carperitide seemed to increase coronary forward flow independent of the collateral flow. Furthermore, the myocardial End/Epi flow ratio was augmented by carperitide (Figure 3), suggesting that carperitide-induced increases in coronary flow is not luxury flow but effective flow to the ischemic myocardium. On the other hand, the present study also showed that carperitide did not increase the myocardial collateral blood flow during myocardial ischemia in the total coronary occlusion model (Table 1), suggesting that carperitide may not increase collateral flow. Further study is needed to study the effects of carperitide on collateral flow in the animal model with less collateral flow in the future. Fifth, carperitide attenuates oxidative stress[26,27] that may contribute to coronary vasodilation in ischemic hearts because oxygen-derived free radicals reduce coronary vasodilation by reducing NO bioavailability.[28,29] However, cardiac NO levels decreased in response to carperitide, arguing against this possibility.

How does carperitide affect NO in ischemic hearts? Our results demonstrate that carperitide does not increase NO production in ischemic hearts. Alternatively, the inhibition of NOS may deactivate downstream ANP receptors because L-NAME attenuates increases in cyclic GMP levels following ANP receptor activation. Several lines of evidence support the idea that NO modulates carperitide activity:[11–14] both factors signal via cyclic GMP and the soluble and particulate guanylate cyclase pathways. It is reported that ANP increases cardiac NOS activity and thus cardiac NO synthesis;[30] the same authors reported that ANP increased NOS activity, but the activation was lower in spontaneously hypertensive rats than Wistar-Kyoto rats.[31] Intriguingly, carperitide significantly decreased NO production in ischemic hearts (Figures 4c and 6c) in the present study. These data seem to be contradictory, but this is not the case. One possible explanation is that cardiac NOS activity may be already saturated in the coronary hypoperfusion model of the present study, and carperitide-induced NO-independent coronary vasodilation may become a major determinant of coronary vascular tone. Another possibility is that these differences may be attributable to the variations in experimental models (normotensive vs. hypertensive hearts and nonischemic vs. ischemic hearts). Whatever the mechanisms are, this study is the first to reveal a relationship between carperitide and endogenous NO in ischemic hearts. At present, however, no available evidence details how the sensitivity of ANP receptors or signal transduction following ANP receptor activation is reduced by inhibiting NOS.

Furthermore, it is reported that ANP may ameliorate endothelial dysfunction by upregulating endothelial NOS (coded by NOS3 gene) and downregulating inducible NOS (coded by NOS2 gene).[32] However, as we used L-NAME, a nonselective NOS inhibitor, to examine the involvement of NOS in the carperitide-induced cardioprotection, we could not clarify what type of NOS is activated in hypoperfused and/or ischemic canine hearts by treatment with carperitide. This would be the next target to elucidate the relationship between carperitide and NO.

Role of NO in carperitide-mediated cardiac function in ischemic hearts

It is reported that NO prevents cellular damages by induction of the rapid recovery to normal pH after ischemia/reperfusion via a guanylyl cyclase/cyclic GMP/protein kinase G (PKG) signaling cascade, and thus inhibits mitochondrial permeability transition (MPT).[33] Yang *et al.*[34] reported that ANP infusion decreased infarct size of the risk area, and this effect was mimicked by a cyclic GMP analog that directly activates PKG and likely by opening of mitochondrial KATP channel and stimulation of downstream kinases. Furthermore, Cohen *et al.*[35] reported that postconditioning prevents mitochondrial permeability transition pore (MPTP) formation by maintaining acidosis during the first minutes of reperfusion. Recently, soluble and particulate guanylate cyclase activator exerts cardioprotective effects via cyclic GMP/PKG signaling cascade and activates phospholamban phosphorylation.[36] Therefore, these myocardioprotective mechanistics of carperitide in addition to the coronary vasodilation may be involved in the cardioprotective effects of carperitide in ischemic heart.

Carperitide limits the infarct size

We showed that carperitide reduces infarct size, and this was also revealed in a previous study.[37] Myocardial infarction is caused by many factors, including free radial generation, platelet aggregation, myocardial calcium ion overload, leukocyte activation and excess catecholamines, each of which is reportedly attenuated by carperitide. Carperitide exerts protective effect of cyclic GMP/PKG signaling pathway during reperfusion in isolated myocytes or isolated hearts on top of the vasodilatory effects of carperitide to reduce cardiac preload and afterload, all of which may mediate cardioprotection. However, even if collateral flow is increased by carperitide, the collateral flow-independent infarct size limitation caused by carperitide largely exists because the infarct size-limiting effect of carperitide is observed even after normalization by the collateral flow (Figure 8b). More importantly, clinical observations have shown that carperitide is cardioprotective against ischemia and reperfusion injury.[10,38]

Clinical implications

Carperitide improves the pathophysiology of acute decompensated HF,[8,9] whereas a recent large clinical trial (ASCEND study) suggested that nesiritide, the recombinant human brain natriuretic peptide (BNP), does not reduce mortality and morbidity in patients with acute decompensated HF.[39] Our group and others have reported that carperitide limits infarct size in humans,[10,38] and the present study showed this cardioprotection may require NO. It is to be noted that nitrate is usually administered to patients with AMI that may enhance the effects of carperitide. If this is the case, it would be important to maintain NO at levels that are sufficient to strengthen the effects of carperitide.

CONFLICT OF INTEREST

The authors declare no conflict of interest.

ACKNOWLEDGEMENTS

We thank Akiko Ogai, Madoka Ihara, Mieko Hayakawa and Yuki Hamada for expert technical assistance. This work was supported by Grants-in-aid from the Ministry of Health, Labor, and Welfare-Japan, Grants-in-aid from the Ministry of Education, Culture, Sports, Science and Technology-Japan and Grants from Japan Heart Foundation and Grants from Japan Cardiovascular Research Foundation.

1 Jessup M, Brozena S. Heart failure. *New Engl J Med* 2003; **348**: 2007–2018.
2 Levy D, Kenchaiah S, Larson MG, Benjamin EJ, Kupka MJ, Ho KK, Murabito JM, Vasan RS. Long-term trends in the incidence of and survival with heart failure. *New Engl J Med* 2002; **347**: 1397–1402.
3 Thom T, Haase N, Rosamond W, Howard VJ, Rumsfeld J, Manolio T, Zheng ZJ, Flegal K, O'Donnell C, Kittner S, Lloyd-Jones D, Goff DC Jr, Hong Y, Adams R, Friday G, Furie K, Gorelick P, Kissela B, Marler J, Meigs J, Roger V, Sidney S, Sorlie P, Steinberger J, Wasserthiel-Smoller S, Wilson M, Wolf P, American Heart Association Statistics Committee and Stroke Statistics Subcommittee. Heart disease and stroke statistics-2006 update: a report from the American Heart Association Statistics Committee and Stroke Statistics Subcommittee. *Circulation* 2006; **113**: e85–e151.
4 Shiba N, Watanabe J, Shinozaki T, Koseki Y, Sakuma M, Kagaya Y, Shirato K. Poor prognosis of Japanese patients with chronic heart failure following myocardial infarction–comparison with nonischemic cardiomyopathy. *Circ J* 2005; **69**: 143–149.
5 Kloner RA, Rezkalla SH. Cardiac protection during acute myocardial infarction: where do we stand in 2004? *J Am Coll Cardiol* 2004; **44**: 276–286.
6 Mukoyama M, Nakao K, Hosoda K, Suga S, Saito Y, Ogawa Y, Shirakami G, Jougasaki M, Obata K, Yasue H, Kambayashi Y, Inouye K, Imura H. Brain natriuretic peptide as a novel cardiac hormone in humans. Evidence for an exquisite dual natriuretic peptide system, atrial natriuretic peptide and brain natriuretic peptide. *J Clin Invest* 1991; **87**: 1402–1412.
7 Nakao K, Yasoda A, Ebihara K, Hosoda K, Mukoyama M. Translational research of novel hormones: lessons from animal models and rare human diseases for common human diseases. *J Mol Med* 2009; **87**: 1029–1039.
8 Rubattu S, Sciarretta S, Valenti V, Stanzione R, Volpe M. Natriuretic peptides: an update on bioactivity, potential therapeutic use, and implication in cardiovascular diseases. *Am J Hypertens* 2008; **21**: 733–741.
9 Nishikimi T, Maeda N, Matsuoka H. The role of natriuretic peptides in cardioprotection. *Cardiovasc Res* 2006; **69**: 318–328.
10 Kitakaze M, Asakura M, Kim J, Shintani Y, Asanuma H, Hamasaki T, Seguchi O, Myoishi M, Minamino T, Ohara T, Nagai Y, Nanto S, Watanabe K, Fukuzawa S, Hirayama A, Nakamura N, Kimura K, Fujii K, Ishihara M, Saito Y, Tomoike H, Kitamura S; J-WIND investigators. Human atrial natriuretic peptide and nicorandil as adjuncts to reperfusion treatment for acute myocardial infarction (J-WIND): two randomised trials. *Lancet* 2007; **370**: 1483–1493.
11 Booz GW. Putting the brakes on cardiac hypertrophy: exploiting the NO-cGMP counter-regulatory system. *Hypertension* 2005; **45**: 341–346.
12 Hussain MB, Hobbs AJ, MacAllister RJ. Autoregulation of nitric oxide-soluble guanylate cyclase-cyclic GMP signalling in mouse thoracic aorta. *Br J Pharmacol* 1999; **128**: 1082–1088.
13 Madhani M, Scotland RS, MacAllister RJ, Hobbs AJ. Vascular natriuretic peptide receptor-linked particulate guanylate cyclases are modulated by nitric oxide-cyclic GMP signalling. *Br J Pharmacol* 2003; **139**: 1289–1296.
14 Sabrane K, Kruse MN, Gazinski A, Kuhn M. Chronic endothelium-dependent regulation of arterial blood pressure by atrial natriuretic peptide: role of nitric oxide and endothelin-1. *Endocrinology* 2009; **150**: 2382–2387.
15 Kitakaze M, Minamino T, Node K, Komamura K, Shinozaki Y, Mori H, Kosaka H, Inoue M, Hori M, Kamada T. Beneficial effects of inhibition of angiotensin converting enzyme on ischemic myocardium during coronary hypoperfusion in dogs. *Circulation* 1995; **92**: 950–961.
16 Kitakaze M, Node K, Minamino T, Komamura K, Funaya H, Shinozaki Y, Chujo M, Mori H, Inoue M, Hori M, Kamada T. Role of activation of protein kinase-C in the infarct size-limiting effect of ischemic preconditioning through activation of ecto-5'-nucleotidase. *Circulation* 1996; **93**: 781–791.
17 Green LC, Wagner DA, Glogowski J, Skipper JS, Wishinok SR. Analysis of nitrate, nitrite and [15 N]nitrate in biological fluid. *Anal Biochem* 1982; **126**: 131–138.
18 Honma M, Satoh T, Takezawa J, Ui M. An ultrasensitive method for the simultaneous determination of cyclic AMP and cyclic GMP in small volume samples from blood and tissue. *Biochem Med* 1977; **18**: 257–273.
19 Lowry Oh, Rosebrough NJ, Farr AL, Randall RJ. Protein measurement with Folin phenol reagent. *J Biol Chem* 1951; **193**: 265–275.
20 Mori H, Haruyama S, Shinozaki Y, Okino H, Iida A, Takanashi R, Sakuma I, Husseini WK, Payne BD, Hoffman JI. New nonradioactive microspheres and more sensitive x-ray fluorescence to measure regional blood flow. *Am J Physiol* 1992; **263**: H1946–H1957.
21 Snedecor GW, Cochran WG. *Statistical Methods,* 6th edn. Iowa State University Press, Ames, IA, 1972, pp 258–298.
22 Winer BJ. *Statistical Principles in Experimental Design,* 2nd edn. McGraw-Hill, New York, 1982, pp 1–907.
23 Calderone A, Thaik CM, Takahashi N, Chang DL, Colucci WS. Nitric oxide, atrial natriuretic peptide, and cyclic GMP inhibit the growth-promoting effects of norepinephrine in cardiac myocytes and fibroblasts. *J Clin Invest* 1998; **101**: 812–818.
24 Kitakaze M, Node K, Minamino T, Kosaka H, Shinozaki Y, Mori H, Inoue M, Hori M, Kamada T. Role of nitric oxide in regulation of coronary blood flow during myocardial ischemia in dogs. *J Am Coll Cardiol* 1996; **27**: 1804–1812.
25 Mtairag el M, Houard X, Rais S, Pasquier C, Oudghiri M, Jacob MP, Meilhac O, Michel JB. Pharmacological potentiation of natriuretic peptide limits polymorphonuclear neutrophil-vascular cell interactions. *Arterioscler Thromb Vasc Biol* 2002; **22**: 1824–1831.

26 Laskowski A, Woodman OL, Cao AH, Drummond GR, Marshall T, Kaye DM, Ritchie RH. Antioxidant actions contribute to the antihypertrophic effects of atrial natriuretic peptide in neonatal rat cardiomyocytes. *Cardiovasc Res* 2006; **72**: 112–123.
27 Shono M, Yoshimura M, Nakayama M, Yamamuro M, Abe K, Suzuki S, Mizuno Y, Sugiyama S, Saito Y, Nakao K, Yasue H, Ogawa H. Predominant effect of A-type natriuretic peptide on reduction of oxidative stress during the treatment of patients with heart failure. *Circ J* 2007; **71**: 1040–1046.
28 Gryglewski RJ, Palmer RMJ, Moncada S. Superoxide anion is involved in the breakdown of endothelial-derived vascular relaxing factor. *Nature* 1986; **320**: 454–456.
29 Kitakaze M, Hori M, Takashima S, Iwai K, Sato H, Inoue M, Kitabatake A, Kamada T. Superoxide dismutase enhances ischemia-induced reactive hyperemic flow and adenosine release in dogs: a role of 5'-nucleotidase activity. *Circ Res* 1992; **71**: 558–566.
30 Costa MA, Elesgaray R, Loria A, Balaszczuk AM, Arranz C. Atrial natriuretic peptide influence on nitric oxide system in kidney and heart. *Regul Pept* 2004; **118**: 151–157.
31 Costa MA, Elesgaray R, Caniffi C, Fellet A, Mac Laughlin M, Arranz C. Role of nitric oxide as a key mediator on cardiovascular actions of atrial natriuretic peptide in spontaneously hypertensive rats. *Am J Physiol Heart Circ Physiol* 2010; **298**: H778–H786.
32 Calderone A. The therapeutic effect of natriuretic peptides in heart failure; differential regulation of endothelial and inducible nitric oxide synthases. *Heart Fail Rev* 2003; **8**: 55–70.
33 Kim JS, Ohshima S, Pediaditakis P, Lemasters JJ. Nitric oxide: a signaling molecule against mitochondrial permeability transition- and pH-dependent cell death after reperfusion. *Free Radic Biol Med* 2004; **37**: 1943–1950.
34 Yang XM, Philipp S, Downey JM, Cohen MV. Atrial natriuretic peptide administered just prior to reperfusion limits infarction in rabbit hearts. *Basic Res Cardiol* 2006; **101**: 311–318.
35 Cohen MV, Yang XM, Downey JM. The pH hypothesis of postconditioning: staccato reperfusion reintroduces oxygen and perpetuates myocardial acidosis. *Circulation* 2007; **115**: 1895–1903.
36 Gorbe A, Giricz Z, Szunyog A, Csont T, Burley DS, Baxter GF, Ferdinandy P. Role of cGMP-PKG signaling in the protection of neonatal rat cardiac myocytes subjected to simulated ischemia/reoxygenation. *Basic Res Cardiol* 2010; **105**: 643–650.
37 Padilla F, Garcia-Dorado D, Agulló L, Barrabés JA, Inserte J, Escalona N, Meyer M, Mirabet M, Pina P, Soler-Soler J. Intravenous administration of the natriuretic peptide urodilatin at low doses during coronary reperfusion limits infarct size in anesthetized pigs. *Cardiovasc Res* 2001; **51**: 592–600.
38 Hayashi M, Tsutamoto T, Wada A, Maeda K, Mabuchi N, Tsutsui T, Horie H, Ohnishi M, Kinoshita M. Intravenous atrial natriuretic peptide prevents left ventricular remodeling in patients with first anterior acute myocardial infarction. *J Am Coll Cardiol* 2001; **37**: 1820–1826.
39 Hernandez Adrian F. Acute study of clinical effectiveness of nesiritide in decompensated heart failure. *Late Breaking Clinical Trial Session of 2010 AHA.*

Noninvasive and quantitative live imaging reveals a potential stress-responsive enhancer in the failing heart

Ken Matsuoka,*,† Yoshihiro Asano,*,†,[1] Shuichiro Higo,*,† Osamu Tsukamoto,† Yi Yan,† Satoru Yamazaki,§ Takashi Matsuzaki,* Hidetaka Kioka,*,† Hisakazu Kato,† Yoshihiro Uno,‡ Masanori Asakura,‖ Hiroshi Asanuma,¶ Tetsuo Minamino,* Hiroyuki Aburatani,# Masafumi Kitakaze,‖ Issei Komuro,* and Seiji Takashima*,†

*Department of Cardiovascular Medicine and †Department of Medical Biochemistry and ‡Laboratory of Reproductive Engineering, Institute of Experimental Animal Sciences, Osaka University Graduate School of Medicine, Suita, Japan; §Department of Cell Biology and ‖Department of Clinical Research and Development, National Cerebral and Cardiovascular Center Research Institute, Suita, Japan; ¶Department of Cardiovascular Science and Technology, Kyoto Prefectural University School of Medicine, Kyoto, Japan; and #Genome Science Division, Research Center for Advanced Science and Technology, University of Tokyo, Tokyo, Japan

ABSTRACT **Recent advances in genome analysis have enabled the identification of numerous distal enhancers that regulate gene expression in various conditions. However, the enhancers involved in pathological conditions are largely unknown because of the lack of *in vivo* quantitative assessment of enhancer activity in live animals. Here, we established a noninvasive and quantitative live imaging system for monitoring transcriptional activity and identified a novel stress-responsive enhancer of *Nppa* and *Nppb*, the most common markers of heart failure. The enhancer is a 650-bp fragment within 50 kb of the *Nppa* and *Nppb* loci. A chromosome conformation capture (3C) assay revealed that this distal enhancer directly interacts with the 5′-flanking regions of *Nppa* and *Nppb*. To monitor the enhancer activity in a live heart, we established an imaging system using the firefly luciferase reporter. Using this imaging system, we observed that the novel enhancer activated the reporter gene in pressure overload-induced failing hearts (failing hearts: 5.7±1.3-fold; sham-surgery hearts: 1.0±0.2-fold; $P<0.001$, repeated-measures ANOVA). This method will be particularly useful for identifying enhancers that function only during pathological conditions.—Matsuoka, K., Asano, Y., Higo, S., Tsukamoto, O., Yan, Y., Yamazaki, S., Matsuzaki, T., Kioka, H., Kato, H., Uno, Y., Asakura, M., Asanuma, H., Minamino, T., Aburatani, H., Kitakaze, M., Komuro, I., and Takashima, S. Noninvasive and quantitative live imaging reveals a potential stress-responsive enhancer in the failing heart. *FASEB J.* 28, 1870–1879 (2014). www.fasebj.org**

Key Words: natriuretic peptide · transcriptional regulation · in vivo assessment

GENE EXPRESSION IS REGULATED through the integrated action of many *cis*-regulatory elements, including core promoters, proximal promoters, distant enhancers, and insulators (1). Several methods have been used to explore the function of *cis*-regulatory elements during a variety of developmental stages (2, 3). However, the identification of gene regulatory elements with pathophysiological roles has been technically difficult because there are few appropriate models for monitoring transcriptional activity in live animals under pathological conditions.

Here, we focused on the regulatory elements that are responsive to heart failure. The natriuretic peptides, atrial natriuretic peptide (ANP) and brain natriuretic peptide (BNP), encoded by the neighboring genes *Nppa* and *Nppb* are activated in the embryonic heart, down-regulated after birth, and then reactivated during heart failure. Both peptides are well-known biomarkers that are strongly induced during heart failure and represent its severity. Cardiologists frequently use these peptides as natriuretic and vasorelaxant agents to treat various clinical conditions (4–8). Many studies have tried to elucidate the mechanisms of their transcriptional regulation because factors that regulate these

Abbreviations: 3C, chromosome conformation capture; ANP, atrial natriuretic peptide; BNP, brain natriuretic peptide; ChIP-seq, chromatin immunoprecipitation sequencing; CMV, cytomegalovirus; CR, conserved region; CTCF, CCCTC-binding factor; H3K4me1, histone H3 monomethylated at lysine 4; H3K4me3, histone H3 trimethylated at lysine 4; PE, phenylephrine; TAC, transverse aortic constriction

[1] Correspondence: Osaka University Graduate School of Medicine, 2-2 Yamadaoka, Suita, Osaka 565–0871, Japan. E-mail: asano@cardiology.med.osaka-u.ac.jp

doi: 10.1096/fj.13-245522

This article includes supplemental data. Please visit *http://www.fasebj.org* to obtain this information.

0892-6638/14/0028-1870 © FASEB

natriuretic peptides are potential therapeutic targets for heart disease (9–14).

Mice transgenic for various loci, including the 5′-flanking regions of the natriuretic peptide genes, have been used to identify the regulatory elements required for transcriptional activation either during heart development or in the diseased heart. These studies reported that the 5′-flanking regions of the natriuretic peptide genes regulated their expression during heart development (9, 10, 13); however, the 5′-flanking regions were not responsible for their specific reactivation in the diseased heart (11, 12). A recent study identified the distal enhancer elements regulating the natriuretic peptide genes in the developing heart by examining cardiac-specific transcription factor binding sites; however, these enhancer elements did not respond to heart failure (14). Therefore, the stress-responsive regulatory elements that function during heart failure have not yet been identified and are potentially located outside the 5′-flanking regions.

In this study, we aimed to identify the novel stress-responsive enhancer elements of the *Nppa* and *Nppb* genes in the failing heart. Furthermore, we established a noninvasive and quantitative live imaging assay to monitor the transcriptional activity of candidate enhancers in the failing heart. *In vivo* live imaging of the firefly luciferase reporter in a single mouse enabled us to analyze the sequential changes in enhancer activity during the progression of heart failure. Combined with a fine mapping technique using epigenetic markers, we identified a 650-bp stress-responsive enhancer that was strongly activated by cardiac hypertrophy and heart failure.

MATERIALS AND METHODS

Animals

All procedures were performed according to the U.S. National Institutes of Health (NIH) Guide for the Care and Use of Laboratory Animals (NIH publication no. 85-23, revised 1996) and were approved by the Animal Experiments Committee, Osaka University (approval no. 21-78-10).

Reagents and antibodies

Phenylephrine (PE) was purchased from Sigma-Aldrich (St. Louis, MO, USA). The anti-RNA polymerase II and anti-histone H3 trimethylated at lysine 4 (H3K4me3) antibodies used for chromatin immunoprecipitation sequencing (ChIP-seq) were kind gifts from Dr. H. Kimura (Graduate School of Frontier Biosciences, Osaka University).

Primary culture of neonatal rat cardiomyocytes

Ventricular myocytes obtained from 1- or 2-d-old Wistar rats were prepared and cultured overnight in Dulbecco's modified Eagle's medium (Sigma-Aldrich) containing 10% FBS, as described previously (15).

Comparative genomics

Genome-wide multiple alignments of the genomic sequences containing the *Nppa* and *Nppb* genes were performed using the University of California Santa Cruz (UCSC) Genome Browser (16); 8 vertebrate species were compared, including mouse (mm9, July 2007), rat (rn4, Nov. 2004), human (hg18, Mar. 2006), orangutan (ponAbe2, July 2007), dog (canFam2, May 2005), horse (equCab1, Jan. 2007), opossum (monDom4, Jan. 2006), and chicken (galGal3, May 2006). We used vertebrate Multiz alignment of DNA sequences (17) to analyze the homology of DNA sequences among mouse and other species. We used the Placental Mammal Basewise Conservation assessed by PhyloP (18) to assess the degree of mammalian conservation. Next, we identified discrete conserved fragments. The transcribed sequences within the conserved set were filtered out using known genes, spliced ESTs, and mRNA annotations obtained from the UCSC genome browser. Finally, we manually curated the data set to remove any additional false positives by visual examination of the UCSC genomic data. We defined the noncoding conserved regions (CRs) that were homologous at least in the human and mouse genomes and at least 1 kb away from the transcription start sites as the enhancer candidates.

ChIP sequencing on mouse heart tissues

Whole hearts were isolated from 8-wk-old C57BL6 mice, perfused rapidly with cold PBS, flash-frozen in liquid nitrogen, homogenized using a sterile tissue grinder, and cross-linked with 0.3% paraformaldehyde. Subsequently, chromatin isolation, sonication, and immunoprecipitation using an anti-RNA polymerase II antibody and an anti-H3K4me3 antibody were performed. The ChIP DNA and input samples were sheared by sonication, end-repaired, ligated to the sequencing adapters, and amplified. The purified ChIP DNA library samples were sequenced using the Illumina Genome Analyzer II (Illumina, Inc., San Diego, CA, USA). Unfiltered sequence reads were aligned to the mouse reference genome [U.S. National Center for Biotechnology Information (NCBI) build 37, mm9] using Bowtie. RNA polymerase II- and H3K4me3-enriched regions were identified using MACS (19) with the default parameters.

Lentiviral enhancer assay

Eleven CRs were PCR amplified from the mouse BAC clone containing the *Nppa* and *Nppb* loci (clone RP23-128E8; BACPAC Resources Center, Children's Hospital Oakland, Oakland, CA, USA; primers and probes are listed in Supplemental Table S1). The PCR fragments were subcloned into the pCR-Blunt II-TOPO vector (Invitrogen, Carlsbad, CA, USA) and recombined into a lentiviral vector encoding the firefly luciferase reporter (pGreenFire Transcriptional Reporter Lentivector; System Biosciences, Mountain View, CA, USA). The lentiviral particles were produced by transfection of 293T cells with the 3 lentiviral packaging plasmids (*i.e.*, pMDLg/pRRE, pRSV-Rev, and pMD2.VSV.G) using Lipofectamine 2000 (Invitrogen). The supernatant from 293T cells containing the lentiviral particles was collected 48 h after transfection, sterilized using a 0.45-μm cellulose acetate filter, and concentrated by centrifugation (Peg-it Virus Precipitation Solution, System Biosciences).

Rat neonatal cardiomyocytes isolated as described above were plated in 96-well plates. The next day, the medium was replaced with a serum-free medium containing the lentiviral vector, and the cells were incubated for 12 h. Subsequently, the cardiomyocytes were exposed to 100 μM PE for 48 h prior to the luciferase assay.

RNA extraction and quantitative RT-PCR

The total RNA was prepared from rat cardiomyocytes, rat cardiac fibroblasts, murine hearts, and murine brains using the RNA-Bee RNA isolation reagent (Tel-Test, Friendswood, TX, USA) and then converted to cDNA using the high-capacity cDNA reverse transcription kit (Applied Biosystems, Foster City, CA, USA), according to the manufacturer's instructions. The quantitative RT-PCR was performed using the TaqMan technology and the StepOnePlus real-time PCR System (Applied Biosystems). All samples were processed in duplicate. The level of each transcript was quantified according to the threshold cycle (C_t) method using GAPDH as an internal control. Inventoried TaqMan gene expression assays were used: *Nppa*, Rn0056661, Mm01255748; *Nppb*, Rn00580641, Mm01255770; *Gapdh*, rodent GAPDH control reagent.

3C analysis

The whole hearts of the mice were isolated, perfused rapidly with cold PBS, flash-frozen in liquid nitrogen, homogenized using a sterile tissue grinder, and fixed with 1% paraformaldehyde. The cross-linked tissues utilized for 3C experiments were subjected to digestion with *Bam*HI following standard protocols (20, 21). The mouse BAC DNA containing *Nppa* and *Nppb* (clone RP23-128E8) was used as a control. The TaqMan real-time PCR was performed using probes near the restriction sites; the primers and probes are listed in Supplemental Table S2.

Transgenic mouse enhancer assay

The candidate enhancer regions were cloned into a vector encoding the minimal CMV promoter driving the luciferase gene as described above. Transgenic mouse embryos were generated by pronuclear injection into the zygotes of BDF1 mice using standard methods. Because black fur attenuates light transmission, albino mice were generated by crossing the transgenic founders to ICR albino mice.

In vivo bioluminescence imaging

Prior to *in vivo* imaging, the mice were anesthetized using isoflurane, and the black mice were shaved from the neck to the lower torso to allow the optimal visualization of fluorescence without interference from the black fur. A D-luciferin solution was injected intraperitoneally (150 mg/kg i.p.) or intravenously (75 mg/kg i.v.). The mice were imaged using an *in vivo* live imaging system (IVIS Lumina II; Caliper Life Sciences, Waltham, MA, USA). For quantification, the bioluminescence light intensity was measured at the region of interest and expressed in relative light units (RLU/min) using Living Image 4.0 (Caliper Life Sciences). To calculate the enhancer activity in the heart, we defined the ratio of heart to brain luciferase intensities as the cardiac-specific enhancer activity.

Transverse aortic constriction (TAC)

Transgenic mice aged 8 wk and weighing 20–25 g were subjected to pressure overload, as described previously (22). Briefly, the chest was entered *via* the second intercostal space at the upper left sternal border. After the arch of the aorta was isolated, a TAC was created using a 7-0 suture tied twice around a 27-gauge needle and the aortic arch, between the innominate and left common carotid arteries. After the suture was tied, the needle was gently removed, yielding 60–80% constriction of the aorta.

PE-induced hypertrophy

Transgenic mice aged 8 wk and weighing 20–25 g were treated with PE (75 mg/kg/d) using an osmotic minipump (Alzet, Cupertino, CA, USA) to induce cardiac hypertrophy, as previously reported (23, 24).

Statistical analysis

Data are expressed as means ± SE. The 2-tailed Student's *t* test and repeated ANOVA were used to analyze differences between the groups. Values of $P < 0.05$ were considered to represent a significant difference.

RESULTS

Identification of candidate enhancers near the *Nppa-Nppb* locus using comparative genomics and ChIP-seq

To identify potential enhancers, we performed a comparative analysis of the genomic sequences of mouse and divergent species and identified CRs that may function as common regulatory sequences (25–27). We defined CRs that were homologous at least in the human and mouse genomes and at least 1 kb away from the transcription start sites of *Nppa* and *Nppb* as the candidate enhancers. First, we analyzed the 50-kb *Nppa-Nppb* locus bounded by the binding sites of 2 CCCTC-binding factors (CTCFs), which can function as insulators (28, 29). Using a genome database (30), we identified 11 CRs, including the *Nppa* and *Nppb* introns in the 50-kb region (**Fig. 1**).

Next, we performed a ChIP-seq analysis on RNA polymerase II and H3K4me3 in the adult mouse heart. We analyzed the epigenetic modifications near the *Nppa* and *Nppb* genes combined with the ChIP-seq analysis using a public database of the adult mouse heart (30). We hypothesized that the normal heart would have activated epigenetic marks because *Nppa* and *Nppb* are expressed, albeit at low levels, in normal conditions. Recent genome-wide studies have determined that enhancers can be defined as DNA sequences bound by the RNA polymerase II and transcriptional coactivator protein p300, and where histone H3 monomethylated at lysine 4 (H3K4me1) accumulates instead of H3K4me3 (31–34). Among the 11 CRs identified, only CR9 coincided with the binding sites of RNA polymerase II and p300, and overlapped with the gene areas modified by H3K4me1, and filled all criteria for the enhancer (Fig. 1). In addition, H3K4me1 modifications in CR9 were only observed in the heart but not in the other organs (Fig. 1 and Supplemental Fig. S1). Therefore, we analyzed the 11 CRs, including CR9, as the most likely distal candidate enhancers for the stress-responsive regulatory regions of the natriuretic peptide genes.

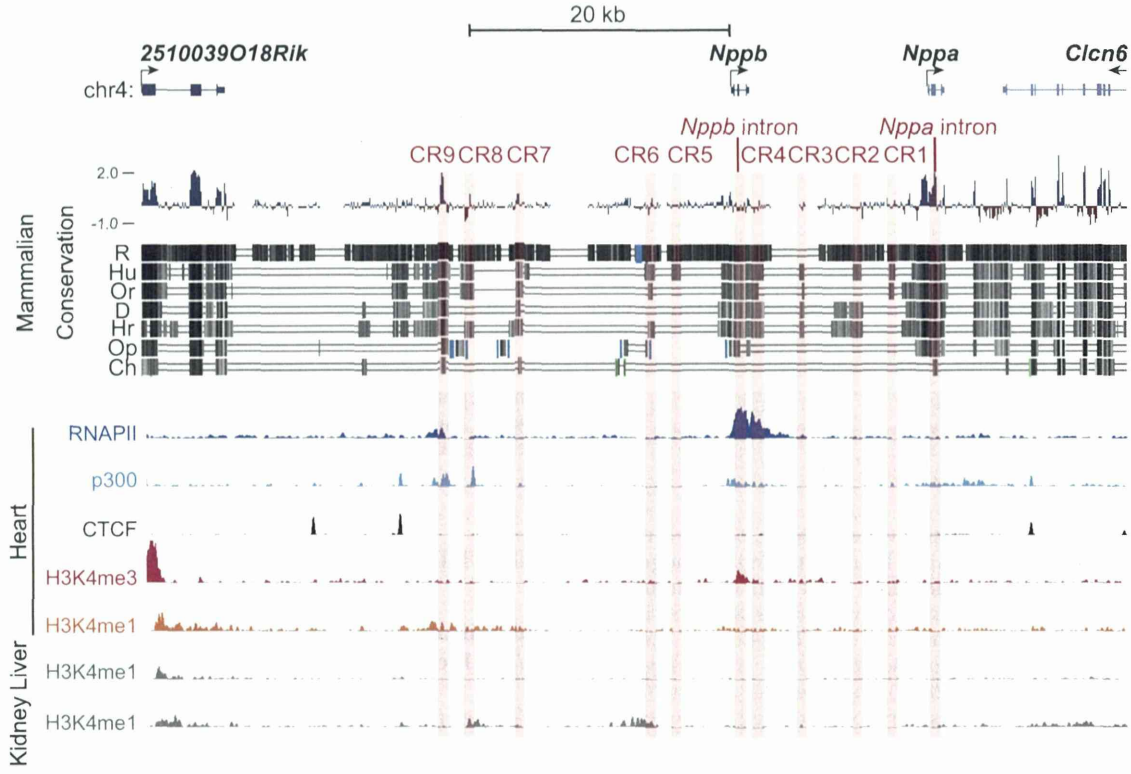

Figure 1. Mammalian evolutionarily conserved regions and ChIP-seq data surrounding the murine *Nppa* and *Nppb* loci. We used an open database on the University of California Santa Cruz (UCSC) Genome Browser to assess the degree of DNA sequence conservation around *Nppa* and *Nppb* gene loci. Blue and red vertical lines, the Placental Mammal Basewise Conservation assessed by PhyloP; black vertical lines, the vertebrate Multiz alignment of DNA sequences among mice and 7 other species (rats, humans, orangutans, dogs, horses, opossums, and chickens). We defined noncoding conserved regions (CRs) that were homologous at least in the human and mouse genomes and at least 1 kb away from the transcription start sites of *Nppa* and *Nppb* as the candidate enhancers. CRs are highlighted as light red vertical bars (CR1-9, *Nppa* intron, and *Nppb* intron). ChIP-seq data for H3K4me1, p300, and CTCF were obtained from an open database of the adult mouse heart. Some CRs coincided with the peaks for H3K4me1, RNA polymerase II, and the transcriptional coactivator protein p300. R, rat; Hu, human; Or, orangutan; D, dog; Hr, horse; Op, opossum; Ch, chicken.

Identification of a distal enhancer element responsive to an α_1-adrenergic receptor agonist

We screened the candidate enhancers for potential stress-responsive regulatory regions. We analyzed the enhancer activity of these 11 CRs after treatment with PE, an α_1-adrenergic receptor agonist, which mimics cardiac overload and induces *Nppa* and *Nppb* expression in cardiomyocytes (35). We confirmed that PE induced the expression of endogenous *Nppa* and *Nppb* specifically in cardiomyocytes but not in cardiac fibroblasts (**Fig. 2*A***). Then, we introduced the 11 CRs with a minimum human cytomegalovirus (CMV) promoter and the luciferase gene into rat cardiomyocytes using a lentiviral vector system.

Among the 11 CRs tested, only CR9, which is located 22 kb upstream from the *Nppb* transcription start site and shows high mammalian conservation score in the Placental Mammal Basewise Conservation by PhyloP (Fig. 2*B*), reproducibly increased the PE-induced luciferase activity by ~5-fold compared to the minimal CMV promoter alone (Fig. 2*C*). However, CR9 did not respond to PE in cardiac fibroblasts (Fig. 2*C*). These results suggest that CR9 is the regulatory element that is responsive to PE specifically in cardiomyocytes.

Long-range physical interaction between the distal enhancer element and the proximal promoters of the *Nppa* and *Nppb* genes

Confirming the looping interactions between distal elements and promoters is one way to demonstrate the transcriptional regulatory activity of distal elements. We performed a 3C assay (20) to comprehensively investigate whether the genomic region containing CR9 moved closer to the *Nppa* or *Nppb* promoter in an adult murine heart treated with a continuous infusion of PE *in vivo*.

The ligation frequencies were quantified by TaqMan real-time PCR using specific primers and probes and were compared to the ligation frequency of noncross-linked *Bam*HI-digested BAC DNA containing the *Nppa-Nppb* locus. We observed that CR9 interacts with both the *Nppa* and *Nppb* promoter regions at a higher frequency relative to other gene areas (Fig. 2*D*); furthermore, PE treatment strengthened these interac-

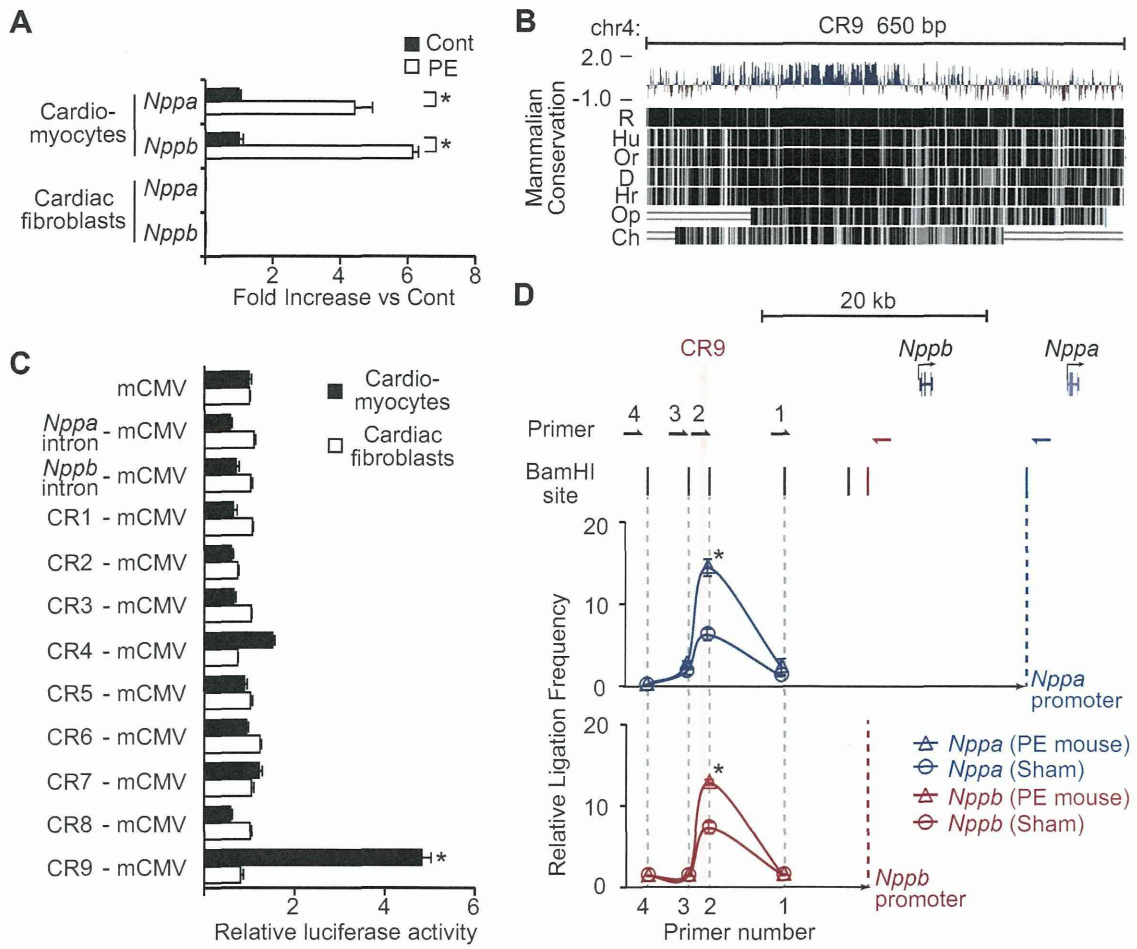

Figure 2. Identification of a distal enhancer element that is responsive to an α_1-adrenergic receptor agonist. *A*) Relative transcript levels of *Nppa* and *Nppb* in rat neonatal cardiomyocytes and cardiac fibroblasts 48 h after treatment with PE (100 μM). Values are means ± SE (n=3 cultures). *$P < 0.01$ *vs.* control; *t* test. *B*) CR9 is a highly conserved genomic region in vertebrates. *C*) Relative luciferase reporter activities of CRs in rat neonatal cardiomyocytes and cardiac fibroblasts 48 h after treatment with PE (100 μM). PE-induced luciferase activity driven by the mCMV promoter was defined as 1. Values are means ± SE (n=5 cultures). *$P < 0.001$ *vs.* mCMV alone; *t* test. *D*) *In vivo* 3C analysis of the murine *Nppa* and *Nppb* loci, showing relative ligation frequencies of each primer to the *Nppa* promoter (blue triangle, mouse with PE treatment; blue circle, mouse without PE) and the *Nppb* promoter (red triangle, mouse with PE treatment; red circle, mouse without PE). Vertical bars and arrows show the positions of *Bam*HI sites and primers. Data were normalized to the amplification value of a *Bam*HI-digested and religated BAC clone, which included the *Nppa* and *Nppb* loci (means ± SE; n=2 hearts). R, rat; Hu, human; Or, orangutan; D, dog; Hr, horse; Op, opossum; Ch, chicken. *$P < 0.05$ *vs.* control; *t* test.

tions (Fig. 2*D*). These results suggest that there is a close proximity between the distal genomic region containing CR9 and the proximal promoters of the *Nppa* and *Nppb* genes in the PE-induced hypertrophic heart.

Establishment of an *in vivo* live imaging system for gene expression in a murine model of heart disease

We confirmed the activity of the newly identified enhancer CR9 in the heart *in vivo*. The conventional histological evaluation of LacZ reporter expression in the heart only provides data at a single time point; therefore, this method cannot be employed for kinetic assessments or time course analyses of reporter expression in a live heart.

To overcome this difficulty, we established a noninvasive and quantitative live imaging system that allowed real-time monitoring of the firefly luciferase reporter. We generated 3 transgenic mouse lines (Tg-line1, Tg-line2, and Tg-line3) in which the CR9 enhancer element and a minimal CMV promoter driving the luciferase reporter gene were introduced into the germline. The live-imaging system detected luciferase expression in the heart, brain, and intestine of the Tg-line1 (**Fig. 3*A***), in the heart, salivary glands, and skin of the Tg-line2 (Supplemental Fig. S2*A*), and in the heart of the Tg-line3 (Supplemental Fig. S2*E*).

To identify the organs in which CR9 functioned as a stress-responsive enhancer, we examined the luciferase reporter expression in each organ by quantitative PCR. Continuous infusion of PE increased the blood pressure and resulted in cardiac hypertrophy (24, 36). The

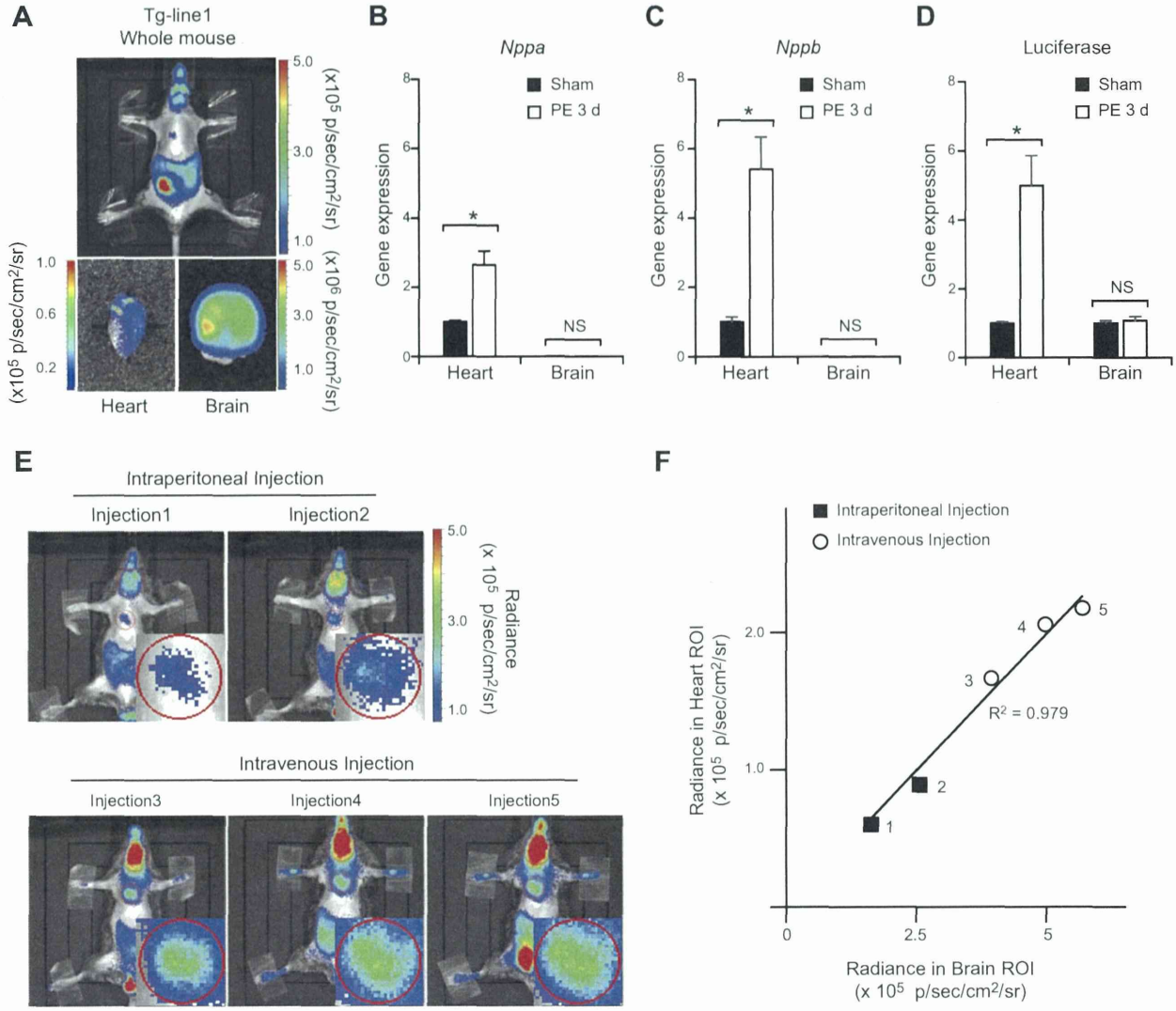

Figure 3. Establishment of an *in vivo* live imaging system for enhancer activity. *A*) Chemiluminescence imaging of CR9 in a mouse of Tg-line1. Top panel: result from whole-animal *in vivo* live imaging. Bottom panels: chemiluminescence images of the heart and brain in the same mouse. *B, C*) Relative transcript levels of *Nppa* and *Nppb* in the ventricular myocardium and brain of CR9 Tg-line1 mice treated with continuous infusion of PE for 3 d. Average transcript level in the ventricular myocardium of preinfused mice was defined as 1 (means ± SE; $n=5$ hearts). $^*P < 0.01$ *vs.* sham-infused mice; *t* test. *D*) Relative transcript levels of luciferase reporter in the ventricular myocardium and brain of the CR9 Tg-line1 mice continuously infused with PE for 3 d. Average transcript level in the ventricular myocardium and brain of preinfused mice was defined as 1. (means ± SE; $n=5$ hearts). $^*P < 0.01$ *vs.* sham-infused mice; *t* test. *E*) Comparison of the chemiluminescence intensities obtained using different luciferin injection methods in a Tg-line1 mouse; injections 1 and 2, intraperitoneal injections (top panels), injections 3, 4, and 5, intravenous injections (bottom panels). Injections were performed ≥4 h apart to eliminate the effect of the previous injection. Inset in each panel shows a magnified image of the heart. *F*) Scatterplots of the chemiluminescence intensities in the heart and brain. Plots indicate the independent experiments shown in each panel in *E*. There is a linear relationship between the expression in the heart and the brain, $R^2 = 0.979$.

expression of endogenous *Nppa* and *Nppb* mRNA increased 3 d after the PE infusion began (Fig. 3*B, C* and Supplemental Fig. S2*B, C, F, G*). Concomitantly, the quantitative PCR analysis of the CR9 luciferase mRNA expression showed enhanced expression in the ventricular myocardium 3 d after the PE infusion (Fig. 3*D* and Supplemental Fig. S2*D, H*). On the other hand, in the brain and the salivary glands where neither *Nppa* nor *Nppb* is highly expressed, the CR9-driven luciferase mRNA expression did not respond to PE (Fig. 3*B–D* and Supplemental Fig. S2*B–D, F–H*). Therefore, the patterns of PE-induced luciferase expression suggest that CR9 is almost exclusively active in the heart. Because the integration sites were random in these three lines, the patterns of luciferase expression depend on CR9 or other enhancers near the integrated sites. The expression of luciferase in the brain of Tg-line1 and salivary glands of Tg-line2, both of which express neither *Nppa* nor *Nppb*, might be driven by other enhancers near the integrated sites.

To evaluate the accuracy and reproducibility of this method, we measured the luminescence in the heart of

a mouse from Tg-line1. In this transgenic line, the brain, intestine, and testis expressed the reporter protein due to positional effects of the insertion site and most likely not due to CR9 activity. Because the luciferase mRNA expression in the brain remained unchanged after PE treatment (Fig. 3*D*), we used the reporter activity in the brain as a control. The absolute luminescence values of the heart were affected by the injection method and the amount of luciferase substrate injected (Fig. 3*E*). However, using brain luminescence as a control, we successfully eliminated the signal variations caused by these differences. The ratio of the luminescence in the heart and brain remained constant within each mouse, independent of the injection method (Fig. 3*F*). Therefore, we defined the ratio of heart to brain luciferase intensities as the cardiac-specific enhancer activity.

Distal enhancer element was activated in the murine model of heart failure

To examine whether the CR9 enhancer was also responsible for gene expression in other pathological conditions, we subjected Tg-line1 mice to heart failure induced by TAC and compared them with sham-surgery mice. This model mimics the heart condition of patients with hypertension who suffer a continuous pressure overload on the heart. The pressure overload by TAC caused potent cardiac hypertrophy at 2 wk postsurgery and reduced cardiac contractility at 3 wk postsurgery (**Fig. 4*A*, *B***), as previously reported (22). The endogenous *Nppa* and *Nppb* expression increased severalfold in the ventricular myocardium 3 wk after the TAC surgery (Fig. 4*C*). The heart to brain luciferase intensity ratio also increased severalfold 3 wk following the TAC surgery (Fig. 4*D*, *E* and Supplemental Fig. S3). However, the heart to brain luciferase intensity ratio of sham-surgery mice did not change after the surgery (Fig. 4*D*, *E* and Supplemental Fig. S3; 3 wk after TAC surgery: 5.7±1.3 fold; 3 wk after sham surgery: 1.0±0.2 fold; $P < 0.001$, repeated ANOVA). These results suggest that CR9 increases transcriptional activity during mechanical pressure overload-induced hypertrophy and subsequent heart failure.

DISCUSSION

Here, we focused on the stress-responsive regulatory elements of *Nppa* and *Nppb* in heart failure. By screening the evolutionarily conserved and epigenetically modified regions around the *Nppa* and *Nppb* gene loci, we identified a 650-bp transcriptional enhancer that was responsive to an α_1-adrenergic receptor agonist *in vitro*. Furthermore, *in vivo* 3C analysis revealed that this distal enhancer directly interacted with the 5′-flanking regions of both *Nppa* and *Nppb*. Using *in vivo* live imaging of luciferase reporter gene expression, we observed that this 650-bp enhancer caused cardiac-specific activation of reporter gene expression during the progression of pressure overload-induced heart failure. Notably, this is the first study to provide a time series analysis for monitoring enhancer activity under pathological conditions in an individual live mouse.

Although numerous approaches have been used to explore the stress-responsive regulatory elements driving gene transcription during heart failure (11, 12, 14), these elements have not yet been identified due to the technical difficulty involved. To detect the elements that are responsive to pathological conditions such as heart failure, it is essential to confirm the activity of the responsive element using a beating heart that remains connected to the systemic cardiovascular system. Therefore, it would be beneficial to establish transgenic mouse lines carrying a reporter plasmid to assess the responsive elements driving the expression of specific genes. However, the creation of multiple stable adult mouse lines to identify these elements is time-consuming.

In this study, we utilized two improved methods for reporter analysis and successfully identified a novel potent enhancer.

First, by performing an enhancer analysis using a lentiviral vector, we accurately identified candidate enhancers in cardiomyocytes and subsequently generated transgenic reporter mice. Previous promoter analyses used electroporation or lipofection to transfect cultured cardiomyocytes with plasmids (37, 38), but the transfection efficiency of these methods in primary cardiomyocytes is too low to accurately measure reporter activity during the stress response. In this study, greater than 90% transduction efficiency of cardiomyocytes was achieved using a lentiviral vector, which enabled us to accurately identify a specific enhancer fragment. Using this method, we efficiently minimized the number of reporter plasmids to be subsequently integrated into the mouse genome to screen for potential enhancers.

Second, by sequentially measuring the enhancer activity in a single live mouse, we collected robust data to assess enhancer activity in the heart *in vivo*. LacZ is not a suitable reporter for this purpose because LacZ activity can only be assessed after animal euthanization. Therefore, we overcame this limitation using the luciferase reporter plasmid. Recent advances in high-sensitivity luminescence imaging have made it possible to evaluate enhancer-driven luciferase activity without operating on the mice. Therefore, we sequentially assessed reporter activity and hemodynamic changes in the same mouse throughout the time course of the development of heart failure. These data were highly reproducible and enabled us to identify an enhancer element that was activated by cardiac overload. Because this method can be applied to any organ, the *in vivo* luciferase reporter assay may be used for assessing the *in vivo* enhancer or promoter activities responsible for clinically important diseases. The noninvasive nature of this method also enabled us to simultaneously assess the hemodynamic and metabolic parameters *in vivo* along with reporter activity. Specifically, the Tg-line1

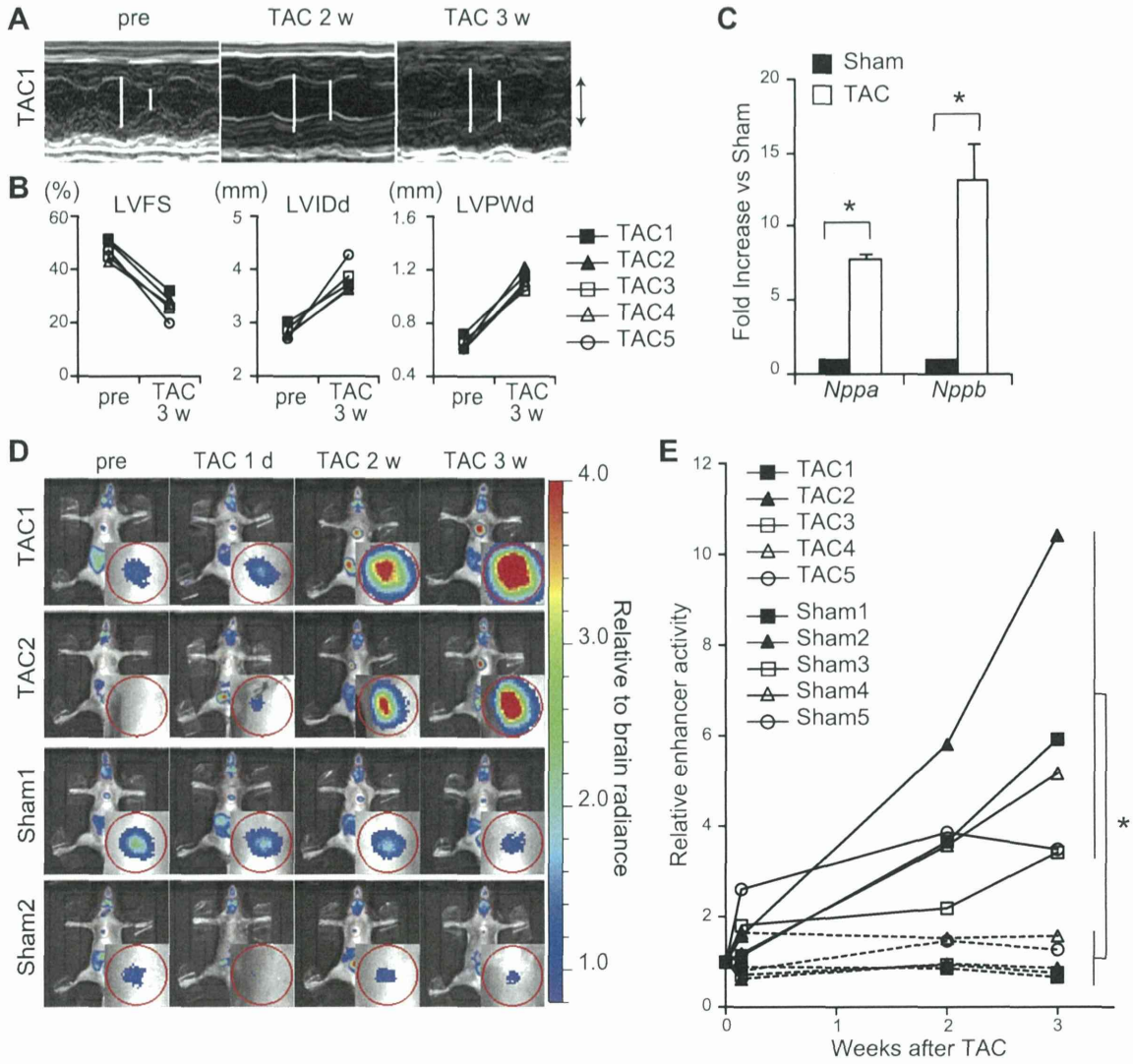

Figure 4. Distal enhancer element is reactivated in the murine model of heart failure. *A*) Representative M-mode echocardiograms in a mouse of Tg-line1 (TAC1) before and after TAC. Open bars indicate maximal left ventricular internal dimension in diastole (LVIDd) and maximal left ventricular internal dimension in systole (LVIDs). Up and down arrows represent 3 mm. *B)* Echocardiographic changes in left ventricular fractional shortening (LVFS), LVIDd, and left ventricular posterior wall thickness in diastole (LVPWd) in 5 mice of Tg-line1 (TAC1-5) before and after TAC. *C*) Relative *Nppa* and *Nppb* transcript levels in the ventricular myocardium 3 wk after the TAC procedure (means ± SE; n=3 hearts). *$P < 0.05$ *vs.* sham-surgery mice; *t* test. *D*) Sequential *in vivo* live imaging of 4 representative Tg-line1 mice before and after TAC or sham surgery at each time point. Top 2 and bottom 2 panels represent sequential imaging data of TAC and sham-surgery mice, respectively. Sequential imaging of the 6 other surgically treated mice is shown in Supplemental Fig. S3. Insets in images show magnified images of the heart. Color scale depends on the ratio relative to brain intensity. *E*) Cardiac-specific enhancer activity plots of 10 Tg-line1 mice (TAC1, TAC2, and Sham1, Sham2, shown in *D*) and TAC3–5 and Sham3–5 shown in Supplemental Fig. S3). Heart to brain luciferase intensity ratio represents the cardiac-specific enhancer activity; enhancer activity in presurgery mice was defined as 1. 3 wk after TAC surgery: 5.7 ± 1.3 fold; 3 wk after sham surgery: 1.0 ± 0.2 fold; means ± SE; $n = 5$. *$P < 0.001$, repeated ANOVA.

mice enabled us to accurately quantify the expression level of the natriuretic peptides. These mice are useful tools for repeatedly assessing the degree of heart failure to screen various cardiovascular drugs.

The integration of activities from multiple enhancers could confer specificity and robustness to transcriptional regulation (1). Warren *et al.* (14) identified the *Nppa* enhancer in the embryonic heart by examining Nkx2-5 binding regions around the *Nppa* locus, but the enhancer did not respond to heart failure. This enhancer does not overlap with CR9 and might regulate *Nppa* expression only during the embryonic stage (14). On the other hand, Horsthuis *et al.* (11) showed that the regulatory region from −27 to +58 kb relative to the transcription start site of *Nppa* was sufficient for *Nppa* gene expression in the failing heart, similar to CR9. However, because this 85-kb regulatory region does not include CR9, *Nppa* may have multiple enhanc-

ers that regulate its expression during heart failure. Furthermore, the length of the 85-kb region poses a challenge for understanding its specific biological role.

This is the first study to provide a time course imaging analysis of enhancer activity using an individual live diseased mouse model. Using this new method, we identified a novel heart enhancer. This method can be widely used for identifying enhancers that regulate transcriptional activity only under pathological conditions. FJ

This research was supported by the Japan Society for the Promotion of Science (JSPS) through the Funding Program for Next Generation World-Leading Researchers (NEXT Program), which was initiated by the Council for Science and Technology Policy (CSTP); grants-in-aid from the Ministry of Health, Labor, and Welfare of Japan; grants-in-aid from the Ministry of Education, Culture, Sports, Science, and Technology of Japan; and grants-in-aid from the Japan Society for the Promotion of Science. This research was also supported by grants from the Japan Heart Foundation, the Japan Cardiovascular Research Foundation, the Japan Medical Association, the Japan Intractable Diseases Research Foundation, the Uehara Memorial Foundation, the Takeda Science Foundation, the Ichiro Kanehara Foundation, the Inoue Foundation for Science, the Mochida Memorial Foundation, a Heart Foundation/Novartis Grant for Research Award on Molecular and Cellular Cardiology, the Japan Foundation of Applied Enzymology, the Naito Foundation, the Banyu Foundation, and Showa Houkoukai. The authors thank Hiroshi Kimura for antibodies, Seitaro Nomura for the ChIP-seq analysis, Saori Ikezawa and Eri Takata for technical assistance, and Yuko Okada and Hiromi Fujii for secretarial support.

REFERENCES

1. Spitz, F., and Furlong, E. E. (2012) Transcription factors: from enhancer binding to developmental control. *Nat. Rev. Genet.* **13,** 613–626
2. Chien, K. R., Domian, I. J., and Parker, K. K. (2008) Cardiogenesis and the complex biology of regenerative cardiovascular medicine. *Science* **322,** 1494–1497
3. Olson, E. N. (2006) Gene regulatory networks in the evolution and development of the heart. *Science* **313,** 1922–1927
4. Burley, D. S., and Baxter, G. F. (2007) B-type natriuretic peptide at early reperfusion limits infarct size in the rat isolated heart. *Basic Res. Cardiol.* **102,** 529–541
5. Holtwick, R., van Eickels, M., Skryabin, B. V., Baba, H. A., Bubikat, A., Begrow, F., Schneider, M. D., Garbers, D. L., and Kuhn, M. (2003) Pressure-independent cardiac hypertrophy in mice with cardiomyocyte-restricted inactivation of the atrial natriuretic peptide receptor guanylyl cyclase-A. *J. Clin. Invest.* **111,** 1399–1407
6. Kitakaze, M., Asakura, M., Kim, J., Shintani, Y., Asanuma, H., Hamasaki, T., Seguchi, O., Myoishi, M., Minamino, T., Ohara, T., Nagai, Y., Nanto, S., Watanabe, K., Fukuzawa, S., Hirayama, A., Nakamura, N., Kimura, K., Fujii, K., Ishihara, M., Saito, Y., Tomoike, H., and Kitamura, S. (2007) Human atrial natriuretic peptide and nicorandil as adjuncts to reperfusion treatment for acute myocardial infarction (J-WIND): two randomised trials. *Lancet* **370,** 1483–1493
7. Li, P., Wang, D., Lucas, J., Oparil, S., Xing, D., Cao, X., Novak, L., Renfrow, M. B., and Chen, Y. F. (2008) Atrial natriuretic peptide inhibits transforming growth factor beta-induced Smad signaling and myofibroblast transformation in mouse cardiac fibroblasts. *Circ. Res.* **102,** 185–192
8. Tamura, N., Ogawa, Y., Chusho, H., Nakamura, K., Nakao, K., Suda, M., Kasahara, M., Hashimoto, R., Katsuura, G., Mukoyama, M., Itoh, H., Saito, Y., Tanaka, I., Otani, H., and Katsuki, M. (2000) Cardiac fibrosis in mice lacking brain natriuretic peptide. *Proc. Natl. Acad. Sci. U. S. A.* **97,** 4239–4244
9. De Lange, F. J., Moorman, A. F., and Christoffels, V. M. (2003) Atrial cardiomyocyte-specific expression of Cre recombinase driven by an Nppa gene fragment. *Genesis* **37,** 1–4
10. Habets, P. E., Moorman, A. F., Clout, D. E., van Roon, M. A., Lingbeek, M., van Lohuizen, M., Campione, M., and Christoffels, V. M. (2002) Cooperative action of Tbx2 and Nkx2.5 inhibits ANF expression in the atrioventricular canal: implications for cardiac chamber formation. *Genes Dev.* **16,** 1234–1246
11. Horsthuis, T., Houweling, A. C., Habets, P. E., de Lange, F. J., el Azzouzi, H., Clout, D. E., Moorman, A. F., and Christoffels, V. M. (2008) Distinct regulation of developmental and heart disease-induced atrial natriuretic factor expression by two separate distal sequences. *Circ. Res.* **102,** 849–859
12. Knowlton, K. U., Rockman, H. A., Itani, M., Vovan, A., Seidman, C. E., and Chien, K. R. (1995) Divergent pathways mediate the induction of ANF transgenes in neonatal and hypertrophic ventricular myocardium. *J. Clin. Invest.* **96,** 1311–1318
13. Small, E. M., and Krieg, P. A. (2003) Transgenic analysis of the atrialnatriuretic factor (ANF) promoter: Nkx2-5 and GATA-4 binding sites are required for atrial specific expression of ANF. *Dev. Biol.* **261,** 116–131
14. Warren, S. A., Terada, R., Briggs, L. E., Cole-Jeffrey, C. T., Chien, W. M., Seki, T., Weinberg, E. O., Yang, T. P., Chin, M. T., Bungert, J., and Kasahara, H. (2011) Differential role of Nkx2-5 in activation of the atrial natriuretic factor gene in the developing versus failing heart. *Mol. Cell. Biol.* **31,** 4633–4645
15. Simpson, P., McGrath, A., and Savion, S. (1982) Myocyte hypertrophy in neonatal rat heart cultures and its regulation by serum and by catecholamines. *Circ. Res.* **51,** 787–801
16. Siepel, A., Bejerano, G., Pedersen, J. S., Hinrichs, A. S., Hou, M., Rosenbloom, K., Clawson, H., Spieth, J., Hillier, L. W., Richards, S., Weinstock, G. M., Wilson, R. K., Gibbs, R. A., Kent, W. J., Miller, W., and Haussler, D. (2005) Evolutionarily conserved elements in vertebrate, insect, worm, and yeast genomes. *Genome Res.* **15,** 1034–1050
17. Blanchette, M., Kent, W. J., Riemer, C., Elnitski, L., Smit, A. F., Roskin, K. M., Baertsch, R., Rosenbloom, K., Clawson, H., Green, E. D., Haussler, D., and Miller, W. (2004) Aligning multiple genomic sequences with the threaded blockset aligner. *Genome Res.* **14,** 708–715
18. Pollard, K. S., Hubisz, M. J., Rosenbloom, K. R., and Siepel, A. (2010) Detection of nonneutral substitution rates on mammalian phylogenies. *Genome Res.* **20,** 110–121
19. Zhang, Y., Liu, T., Meyer, C. A., Eeckhoute, J., Johnson, D. S., Bernstein, B. E., Nusbaum, C., Myers, R. M., Brown, M., Li, W., and Liu, X. S. (2008) Model-based analysis of ChIP-Seq (MACS). *Genome Biol.* **9,** R137
20. Dekker, J., Rippe, K., Dekker, M., and Kleckner, N. (2002) Capturing chromosome conformation. *Science* **295,** 1306–1311
21. Hagege, H., Klous, P., Braem, C., Splinter, E., Dekker, J., Cathala, G., de Laat, W., and Forne, T. (2007) Quantitative analysis of chromosome conformation capture assays (3C-qPCR). *Nat. Protoc.* **2,** 1722–1733
22. Liao, Y., Ishikura, F., Beppu, S., Asakura, M., Takashima, S., Asanuma, H., Sanada, S., Kim, J., Ogita, H., Kuzuya, T., Node, K., Kitakaze, M., and Hori, M. (2002) Echocardiographic assessment of LV hypertrophy and function in aortic-banded mice: necropsy validation. *Am. J. Physiol. Heart Circ. Physiol.* **282,** H1703–H1708
23. Saadane, N., Alpert, L., and Chalifour, L. E. (1999) Expression of immediate early genes, GATA-4, and Nkx-2.5 in adrenergic-induced cardiac hypertrophy and during regression in adult mice. *Brit. J. Pharmacol.* **127,** 1165–1176
24. Vecchione, C., Fratta, L., Rizzoni, D., Notte, A., Poulet, R., Porteri, E., Frati, G., Guelfi, D., Trimarco, V., Mulvany, M. J., Agabiti-Rosei, E., Trimarco, B., Cotecchia, S., and Lembo, G. (2002) Cardiovascular influences of $\alpha 1\beta$-adrenergic receptor defect in mice. *Circulation* **105,** 1700–1707
25. Nobrega, M. A., Ovcharenko, I., Afzal, V., and Rubin, E. M. (2003) Scanning human gene deserts for long-range enhancers. *Science* **302,** 413
26. Thomas, J. W., Touchman, J. W., Blakesley, R. W., Bouffard, G. G., Beckstrom-Sternberg, S. M., Margulies, E. H., Blanchette, M., Siepel, A. C., Thomas, P. J., McDowell, J. C., Maskeri, B., Hansen, N. F., Schwartz, M. S., Weber, R. J., Kent, W. J.,

Karolchik, D., Bruen, T. C., Bevan, R., Cutler, D. J., Schwartz, S., Elnitski, L., Idol, J. R., Prasad, A. B., Lee-Lin, S. Q., Maduro, V. V., Summers, T. J., Portnoy, M. E., Dietrich, N. L., Akhter, N., Ayele, K., Benjamin, B., Cariaga, K., Brinkley, C. P., Brooks, S. Y., Granite, S., Guan, X., Gupta, J., Haghighi, P., Ho, S. L., Huang, M. C., Karlins, E., Laric, P. L., Legaspi, R., Lim, M. J., Maduro, Q. L., Masiello, C. A., Mastrian, S. D., McCloskey, J. C., Pearson, R., Stantripop, S., Tiongson, E. E., Tran, J. T., Tsurgeon, C., Vogt, J. L., Walker, M. A., Wetherby, K. D., Wiggins, L. S., Young, A. C., Zhang, L. H., Osoegawa, K., Zhu, B., Zhao, B., Shu, C. L., De Jong, P. J., Lawrence, C. E., Smit, A. F., Chakravarti, A., Haussler, D., Green, P., Miller, W., and Green, E. D. (2003) Comparative analyses of multi-species sequences from targeted genomic regions. *Nature* **424,** 788–793

27. Woolfe, A., Goodson, M., Goode, D. K., Snell, P., McEwen, G. K., Vavouri, T., Smith, S. F., North, P., Callaway, H., Kelly, K., Walter, K., Abnizova, I., Gilks, W., Edwards, Y. J., Cooke, J. E., and Elgar, G. (2005) Highly conserved non-coding sequences are associated with vertebrate development. *PLoS Biol.* **3,** e7
28. Bell, A. C., West, A. G., and Felsenfeld, G. (1999) The protein CTCF is required for the enhancer blocking activity of vertebrate insulators. *Cell* **98,** 387–396
29. Felsenfeld, G., Burgess-Beusse, B., Farrell, C., Gaszner, M., Ghirlando, R., Huang, S., Jin, C., Litt, M., Magdinier, F., Mutskov, V., Nakatani, Y., Tagami, H., West, A., and Yusufzai, T. (2004) Chromatin boundaries and chromatin domains. *Cold Spring Harb. Symp. Quant. Biol.* **69,** 245–250
30. Shen, Y., Yue, F., McCleary, D. F., Ye, Z., Edsall, L., Kuan, S., Wagner, U., Dixon, J., Lee, L., Lobanenkov, V. V., and Ren, B. (2012) A map of the cis-regulatory sequences in the mouse genome. *Nature* **488,** 116–120
31. Birney, E., Stamatoyannopoulos, J. A., Dutta, A., Guigo, R., Gingeras, T. R., Margulies, E. H., Weng, Z., Snyder, M., Dermitzakis, E. T., Thurman, R. E., Kuehn, M. S., Taylor, C. M., Neph, S., Koch, C. M., Asthana, S., Malhotra, A., Adzhubei, I., Greenbaum, J. A., Andrews, R. M., Flicek, P., Boyle, P. J., Cao, H., Carter, N. P., Clelland, G. K., Davis, S., Day, N., Dhami, P., Dillon, S. C., Dorschner, M. O., Fiegler, H., Giresi, P. G., Goldy, J., Hawrylycz, M., Haydock, A., Humbert, R., James, K. D., Johnson, B. E., Johnson, E. M., Frum, T. T., Rosenzweig, E. R., Karnani, N., Lee, K., Lefebvre, G. C., Navas, P. A., Neri, F., Parker, S. C., Sabo, P. J., Sandstrom, R., Shafer, A., Vetrie, D., Weaver, M., Wilcox, S., Yu, M., Collins, F. S., Dekker, J., Lieb, J. D., Tullius, T. D., Crawford, G. E., Sunyaev, S., Noble, W. S., Dunham, I., Denoeud, F., Reymond, A., Kapranov, P., Rozowsky, J., Zheng, D., Castelo, R., Frankish, A., Harrow, J., Ghosh, S., Sandelin, A., Hofacker, I. L., Baertsch, R., Keefe, D., Dike, S., Cheng, J., Hirsch, H. A., Sekinger, E. A., Lagarde, J., Abril, J. F., Shahab, A., Flamm, C., Fried, C., Hackermuller, J., Hertel, J., Lindemeyer, M., Missal, K., Tanzer, A., Washietl, S., Korbel, J., Emanuelsson, O., Pedersen, J. S., Holroyd, N., Taylor, R., Swarbreck, D., Matthews, N., Dickson, M. C., Thomas, D. J., Weirauch, M. T., Gilbert, J., Drenkow, J., Bell, I., Zhao, X., Srinivasan, K. G., Sung, W. K., Ooi, H. S., Chiu, K. P., Foissac, S., Alioto, T., Brent, M., Pachter, L., Tress, M. L., Valencia, A., Choo, S. W., Choo, C. Y., Ucla, C., Manzano, C., Wyss, C., Cheung, E., Clark, T. G., Brown, J. B., Ganesh, M., Patel, S., Tammana, H., Chrast, J., Henrichsen, C. N., Kai, C., Kawai, J., Nagalakshmi, U., Wu, J., Lian, Z., Lian, J., Newburger, P., Zhang, X., Bickel, P., Mattick, J. S., Carninci, P., Hayashizaki, Y., Weissman, S., Hubbard, T., Myers, R. M., Rogers, J., Stadler, P. F., Lowe, T. M., Wei, C. L., Ruan, Y., Struhl, K., Gerstein, M., Antonarakis, S. E., Fu, Y., Green, E. D., Karaoz, U., Siepel, A., Taylor, J., Liefer, L. A., Wetterstrand, K. A., Good, P. J., Feingold, E. A., Guyer, M. S., Cooper, G. M., Asimenos, G., Dewey, C. N., Hou, M., Nikolaev, S., Montoya-Burgos, J. I., Loytynoja, A., Whelan, S., Pardi, F., Massingham, T., Huang, H., Zhang, N. R., Holmes, I., Mullikin, J. C., Ureta-Vidal, A., Paten, B., Seringhaus, M., Church, D., Rosenbloom, K., Kent, W. J., Stone, E. A., Batzoglou, S., Goldman, N., Hardison, R. C., Haussler, D., Miller, W., Sidow, A., Trinklein, N. D., Zhang, Z. D., Barrera, L., Stuart, R., King, D. C., Ameur, A., Enroth, S., Bieda, M. C., Kim, J., Bhinge, A. A., Jiang, N., Liu, J., Yao, F., Vega, V. B., Lee, C. W., Ng, P., Shahab, A., Yang, A., Moqtaderi, Z., Zhu, Z., Xu, X., Squazzo, S., Oberley, M. J., Inman, D., Singer, M. A., Richmond, T. A., Munn, K. J., Rada-Iglesias, A., Wallerman, O., Komorowski, J., Fowler, J. C., Couttet, P., Bruce, A. W., Dovey, O. M., Ellis, P. D., Langford, C. F., Nix, D. A., Euskirchen, G., Hartman, S., Urban, A. E., Kraus, P., Van Calcar, S., Heintzman, N., Kim, T. H., Wang, K., Qu, C., Hon, G., Luna, R., Glass, C. K., Rosenfeld, M. G., Aldred, S. F., Cooper, S. J., Halees, A., Lin, J. M., Shulha, H. P., Zhang, X., Xu, M., Haidar, J. N., Yu, Y., Ruan, Y., Iyer, V. R., Green, R. D., Wadelius, C., Farnham, P. J., Ren, B., Harte, R. A., Hinrichs, A. S., Trumbower, H., Clawson, H., Hillman-Jackson, J., Zweig, A. S., Smith, K., Thakkapallayil, A., Barber, G., Kuhn, R. M., Karolchik, D., Armengol, L., Bird, C. P., de Bakker, P. I., Kern, A. D., Lopez-Bigas, N., Martin, J. D., Stranger, B. E., Woodroffe, A., Davydov, E., Dimas, A., Eyras, E., Hallgrimsdottir, I. B., Huppert, J., Zody, M. C., Abecasis, G. R., Estivill, X., Bouffard, G. G., Guan, X., Hansen, N. F., Idol, J. R., Maduro, V. V., Maskeri, B., McDowell, J. C., Park, M., Thomas, P. J., Young, A. C., Blakesley, R. W., Muzny, D. M., Sodergren, E., Wheeler, D. A., Worley, K. C., Jiang, H., Weinstock, G. M., Gibbs, R. A., Graves, T., Fulton, R., Mardis, E. R., Wilson, R. K., Clamp, M., Cuff, J., Gnerre, S., Jaffe, D. B., Chang, J. L., Lindblad-Toh, K., Lander, E. S., Koriabine, M., Nefedov, M., Osoegawa, K., Yoshinaga, Y., Zhu, B., and de Jong, P. J. (2007) Identification and analysis of functional elements in 1% of the human genome by the ENCODE pilot project. *Nature* **447,** 799–816
32. Blow, M. J., McCulley, D. J., Li, Z., Zhang, T., Akiyama, J. A., Holt, A., Plajzer-Frick, I., Shoukry, M., Wright, C., Chen, F., Afzal, V., Bristow, J., Ren, B., Black, B. L., Rubin, E. M., Visel, A., and Pennacchio, L. A. (2010) ChIP-Seq identification of weakly conserved heart enhancers. *Nat. Genet.* **42,** 806–810
33. Koch, F., Jourquin, F., Ferrier, P., and Andrau, J. C. (2008) Genome-wide RNA polymerase II: not genes only!. *Trends Biochem. Sci.* **33,** 265–273
34. Szutorisz, H., Dillon, N., and Tora, L. (2005) The role of enhancers as centres for general transcription factor recruitment. *Trends Biochem. Sci.* **30,** 593–599
35. Sei, C. A., Irons, C. E., Sprenkle, A. B., McDonough, P. M., Brown, J. H., and Glembotski, C. C. (1991) The α-adrenergic stimulation of atrial natriuretic factor expression in cardiac myocytes requires calcium influx, protein kinase C, and calmodulin-regulated pathways. *J. Biol. Chem.* **266,** 15910–15916
36. Iaccarino, G., Dolber, P. C., Lefkowitz, R. J., and Koch, W. J. (1999) Bβ-adrenergic receptor kinase-1 levels in catecholamine-induced myocardial hypertrophy: regulation by beta- but not alpha1-adrenergic stimulation. *Hypertension* **33,** 396–401
37. Seidman, C. E., Wong, D. W., Jarcho, J. A., Bloch, K. D., and Seidman, J. G. (1988) *Cis*-acting sequences that modulate atrial natriuretic factor gene expression. *Proc. Natl. Acad. Sci. U. S. A.* **85,** 4104–4108
38. Thuerauf, D. J., and Glembotski, C. C. (1997) Differential effects of protein kinase C, Ras, and Raf-1 kinase on the induction of the cardiac B-type natriuretic peptide gene through a critical promoter-proximal M-CAT element. *J. Biol. Chem.* **272,** 7464–7472

Received for publication November 12, 2013.
Accepted for publication January 2, 2014.

Impact of cardiac support device combined with slow-release prostacyclin agonist in a canine ischemic cardiomyopathy model

Yasuhiko Kubota, MD,[a] Shigeru Miyagawa, MD, PhD,[a] Satsuki Fukushima, MD, PhD,[a] Atsuhiro Saito, PhD,[a] Hiroshi Watabe, PhD,[b] Takashi Daimon, PhD,[c] Yoshiki Sakai, PhD,[a] Toshiaki Akita, MD, PhD,[d] and Yoshiki Sawa, MD, PhD[a]

Background: The cardiac support device supports the heart and mechanically reduces left ventricular (LV) diastolic wall stress. Although it has been shown to halt LV remodeling in dilated cardiomyopathy, its therapeutic efficacy is limited by its lack of biological effects. In contrast, the slow-release synthetic prostacyclin agonist ONO-1301 enhances reversal of LV remodeling through biological mechanisms such as angiogenesis and attenuation of fibrosis. We therefore hypothesized that ONO-1301 plus a cardiac support device might be beneficial for the treatment of ischemic cardiomyopathy.

Methods: Twenty-four dogs with induced anterior wall infarction were assigned randomly to 1 of 4 groups at 1 week postinfarction as follows: cardiac support device alone, cardiac support device plus ONO-1301 (hybrid therapy), ONO-1301 alone, or sham control.

Results: At 8 weeks post-infarction, LV wall stress was reduced significantly in the hybrid therapy group compared with the other groups. Myocardial blood flow, measured by positron emission tomography, and vascular density were significantly higher in the hybrid therapy group compared with the cardiac support device alone and sham groups. The hybrid therapy group also showed the least interstitial fibrosis, the greatest recovery of LV systolic and diastolic functions, assessed by multidetector computed tomography and cardiac catheterization, and the lowest plasma N-terminal pro-B-type natriuretic peptide levels ($P < .05$).

Conclusions: The combination of a cardiac support device and the prostacyclin agonist ONO-1301 elicited a greater reversal of LV remodeling than either treatment alone, suggesting the potential of this hybrid therapy for the clinical treatment of ischemia-induced heart failure. (J Thorac Cardiovasc Surg 2014;147:1081-7)

Left ventricular (LV) remodeling in ischemic and nonischemic dilated cardiomyopathy is characterized by progressive dilatation and dysfunction of the left ventricle, leading to severe heart failure.[1,2] The cardiac support device is a mesh net designed to reduce diastolic ventricular wall stress by mechanical means and thus prevent LV dilatation. It has been shown to halt LV remodeling in dilated cardiomyopathy in preclinical studies.[3-5] Clinical trials undertaken on the basis of these favorable results showed beneficial effects on LV remodeling, including significantly decreased LV end-systolic (LVESV) and end-diastolic volumes (LVEDV), and a significant improvement in New York Heart Association functional class.[6-8] However, despite these positive effects, the device has not been associated with reductions in mortality and has not been approved for clinical use.[9]

The synthetic prostacyclin agonist ONO-1301 acts as a myocardial regenerative biological drug to enhance reversal of LV remodeling.[10-12] The beneficial effects of ONO-1301 on the heart are mediated by up-regulation of angiogenic and antifibrotic molecules, such as hepatocyte growth factor (HGF), vascular endothelial growth factor (VEGF), and stromal cell–derived factor-1 (SDF-1).[10-12] This mechanism has been shown to result in the active suppression of ischemic and fibrotic changes in the myocardium.[10-12]

We hypothesized that the biological effects of the slow-release form of the synthetic prostacyclin agonist ONO-1301 might complement the mechanical effects of the cardiac support device, thus enhancing its therapeutic effects in ischemic cardiomyopathy.

MATERIALS AND METHODS

All animals used in this study received care in compliance with the Guide for the Care and Use of Laboratory Animals (National Institutes of Health publication no. 85-23, revised 1996).

Animal Treatment

A total of 28 beagles (Oriental Yeast, Co, Ltd, Tokyo, Japan) weighing 9 to 11 kg were used. General anesthesia was administered with intramuscular ketamine (10 mg/kg) and intravenous propofol (5 mg/kg) for induction,

From the Department of Cardiovascular Surgery,[a] Department of Molecular Imaging in Medicine,[b] Osaka University Graduate School of Medicine, Osaka, Japan; Department of Biostatistics,[c] Hyogo College of Medicine, Hyogo, Japan; Department of Cardiovascular Surgery,[d] Kanazawa Medical University, Ishikawa, Japan.

Supported by the New Energy and Industrial Technology Organization and the Japan Society for the Promotion of Science Core-to-Core Program.

Disclosures: Authors have nothing to disclose with regard to commercial support.

Received for publication Feb 12, 2013; revisions received May 9, 2013; accepted for publication May 16, 2013; available ahead of print Oct 15, 2013.

Address for reprints: Yoshiki Sawa, MD, PhD, Department of Cardiovascular Surgery, Osaka University Graduate School of Medicine, 565-0871, 2-2 Yamadaoka, Suita, Osaka, Japan (E-mail: sawa-p@surg1.med.osaka-u.ac.jp).

0022-5223/$36.00

http://dx.doi.org/10.1016/j.jtcvs.2013.05.035

ET/BS

Abbreviations and Acronyms

ANOVA = analysis of variance
dp/dt = delta pressure/delta time
Ees = end-systolic elastance
HGF = hepatocyte growth factor
LV = left ventricular
LVEDV = left ventricular end-diastolic volume
LVESV = left ventricular end-systolic volume
MDCT = multidetector computed tomography
MI = myocardial infarction
NT-proBNP = amino-terminal pro-brain natriuretic peptide
SDF-1 = stromal cell–derived factor-1
VEGF = vascular endothelial growth factor

and inhaled sevoflurane (1%–2%) for subsequent maintenance, with endotracheal intubation and mechanical ventilator support. After completion of the experiments, the animals were killed under general anesthesia, using an overdose of intravenous sodium pentobarbital (18 mg/kg) to achieve complete sedation, followed by administration of an intravenous potassium-based solution.

Myocardial Infarction Induction

With the animals under general anesthesia, a minimal left thoracotomy was performed through the fifth intercostal space, and the heart was exposed by pericardiotomy. The left descending artery and diagonal vessels were ligated both proximally and distally using 5-0 polypropylene sutures to produce an anterior myocardial infarction (MI). Akinesis of the anterior wall was confirmed by epicardial echocardiography and the chest was closed in layers. The animals were allowed to recover.

Cardiac Support Device

The cardiac support device (0.9–1.0 g), made from polyglycolic acid (Nipro Corporation, Osaka, Japan), was designed on the basis of data obtained from multidetector computed tomography (MDCT) and a heart excised at 1 week postinfarction.

Treatments

The animals were assigned randomly to 1 of 4 groups at 1 week after infarct induction as follows: cardiac support device alone, cardiac support device plus ONO-1301 (hybrid therapy), ONO-1301 alone, or sham control group. In the cardiac support device alone group, 2 sheets of atelocollagen (50 × 50 mm) (Integran; Nippon Zoki Pharmaceutical Co, Ltd, Osaka, Japan) immersed in suspended polylactic and glycolic acid (10 mg/kg) were fixed on the whole surface of the ventricles and the cardiac support device was placed as described previously.[3-5] The same procedure was used in the hybrid therapy group, with the addition of ONO-1301[10-12] (10 mg/kg) (ONO Pharmaceutical Co, Ltd, Osaka, Japan) instead of the polylactic and glycolic acid. In the ONO-1301 alone group, 2 sheets of atelocollagen (50 × 50 mm) immersed in suspended ONO-1301 (10 mg/kg) were fixed on the whole surface of the ventricles. The sham group was subjected to the same procedures as the ONO-1301 alone group, except for the use of polylactic and glycolic acid instead of ONO-1301.

Transthoracic Echocardiography

Transthoracic echocardiography was performed using a 5.0-MHz transducer (Altida; Toshiba Medical Systems Corporation, Tochigi, Japan) for 2-dimensional speckle-tracking echocardiography under general anesthesia. The data were analyzed using 2-dimensional Wall Motion Tracking software (Toshiba Medical Systems Corporation) as previously described.[13]

MDCT

Electrocardiography-gated MDCT was performed using a 16-row MDCT scanner (SOMATOM Emotion 16-Slice Configuration; Siemens, Munich, Germany) during an end-expiratory breath-hold under general anesthesia. MDCT was performed after intravenous injection of 30 mL of nonionic contrast medium (Iomeron; Bracco, Milan, Italy). All images were analyzed on a workstation (AZE VirtualPlace Lexus64; AZE, Tokyo, Japan). LVEDV and LVESV, LV ejection fraction, LV end-diastolic and end-systolic sphericity indices, and LV/right ventricular end-diastolic and end-systolic diameter values were obtained from the workstation.

Cardiac Catheterization

Under general anesthesia, a 3F micromanometer-tipped catheter (SPR-249; Millar Instruments, Houston, Tex) was inserted through the ventricular apex via a left thoracotomy to measure hemodynamic parameters and cardiac functions, including end-systolic pressure and end-diastolic pressure, delta pressure/delta time (dp/dt) maximum, dp/dt minimum, end-systolic elastance (Ees), and the time constant of relaxation in the left and right ventricles. LV volume was altered by occluding the inferior vena cava with tape via a left thoracotomy.

Wall Stress Calculation

LV wall stress was evaluated using specifically developed software (YD, Ltd, Tokyo, Japan) on an off-line personal computer. Global end-systolic and end-diastolic wall stresses were calculated on the basis of the data obtained from MDCT and cardiac catheterization.[14]

Cardiac Positron Emission Tomography

^{13}N-ammonia (200–300 MBq) positron emission tomography (PET) was performed using a HeadtomeV/SET2400W (Shimadzu, Co, Kyoto, Japan) under general anesthesia. Myocardial blood flow was quantitated using PMOD software (version 3.2) (PMOD Technologies, Ltd, Zurich, Switzerland) and divided into 17 segments as recommended by the American Heart Association.

Histologic Analysis

Paraffin-embedded transverse sections of the excised hearts were stained with periodic acid-Schiff to measure the short-axis diameter of the myocytes, and with Masson trichrome to assess the extent of fibrosis. The sections were immunostained with anti-CD31 antibody in LSAB kits (DakoCytomation, Glostrup, Denmark). Myocyte diameters and vascular density were measured in 10 different randomly selected fields using a Biorevo BZ-9000 fluorescence microscope (Keyence, Osaka, Japan), and percentage fibrosis was calculated using MetaMorph software (Molecular Devices, Tokyo, Japan).

Real-Time Polymerase Chain Reaction

Total RNA extracted from cardiac tissue was reverse-transcribed using TaqMan reverse transcription reagents (Applied Biosystems, Foster City, Calif), and assayed using the ABI PRISM 7700 (Applied Biosystems). The average copy number of gene transcripts was normalized to that of glyceraldehyde 3-phosphate dehydrogenase for each sample.

Statistical Analysis

All statistical analyses were performed using JMP software (JMP9; SAS institute, Inc, Cary, NC). Results are presented as the mean ± standard deviation. Cardiac catheterization and histologic data were compared by 1-way analysis of variance (ANOVA). MDCT, echocardiography, wall stress, and amino-terminal pro-brain natriuretic peptide (NT-proBNP)

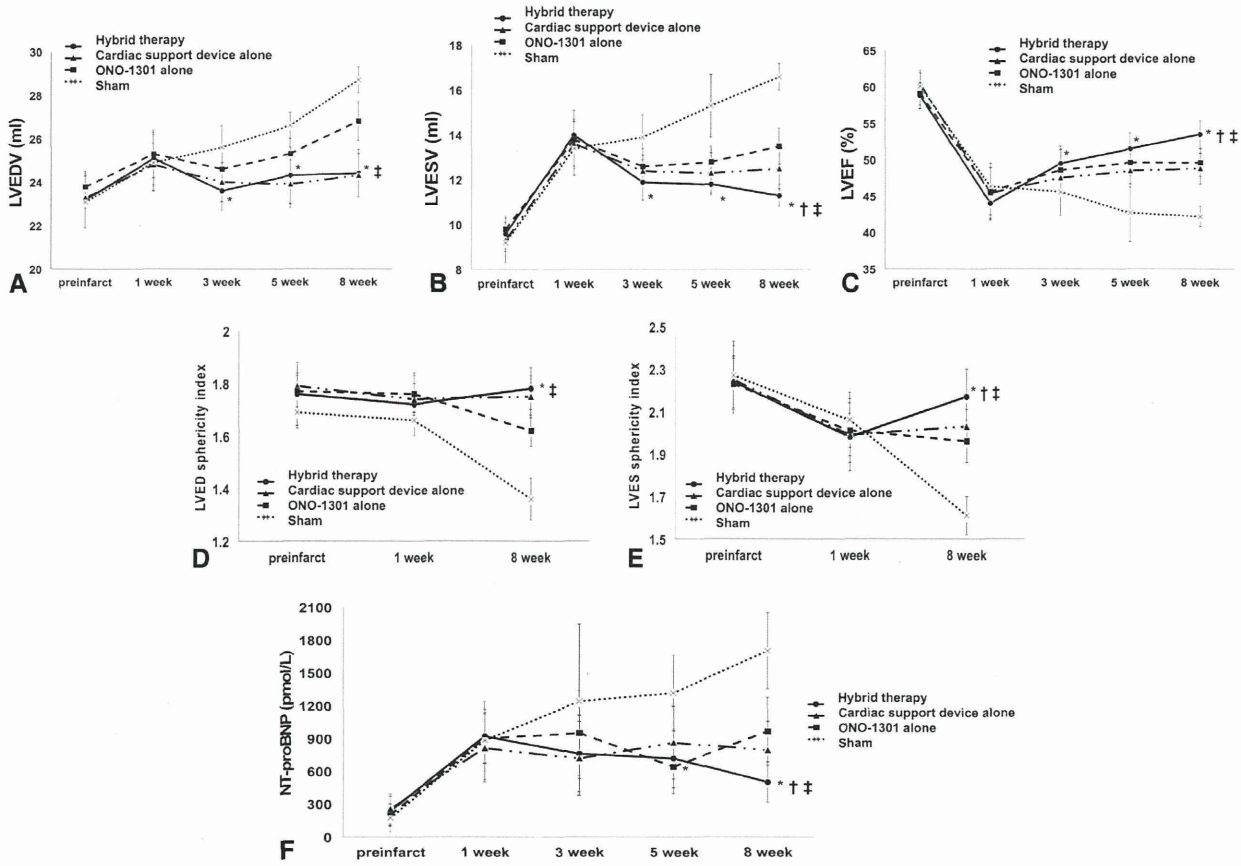

FIGURE 1. MDCT analysis. A, Changes in LVEDV. B, Changes in LVESV. C, Changes in LV ejection fraction. D, Changes in left ventricular end-diastolic and, (E) end-systolic sphericity indices. F, Changes in NT-proBNP. Hybrid therapy is shown by *circles with a solid line*, a cardiac support device alone is shown by *triangles with a dashed/dotted line*, ONO-1301 alone is shown by *squares with a dashed line*, and sham is shown by *crosses with a dotted line*. *$P < .05$ versus corresponding sham, †$P < .05$ versus corresponding cardiac support device alone, ‡$P < .05$ versus corresponding ONO-1301 alone. *LV sphericity index*, LV long-axis diameter/LV short-axis diameter. *LVEDV*, Left ventricular end-diastolic volume; *LVESV*, left ventricular end-systolic volume; *NT-proBNP*, amino-terminal pro-brain natriuretic peptide.

data were compared by repeated ANOVA, using values obtained by subtracting the values at 1 week postinfarction from the values at each time point. Significant differences shown by ANOVA were subjected to post hoc analysis with Bonferroni correction. Sample size justification was not performed. A P value less than .05 was considered statistically significant.

RESULTS

Procedure-Related Morbidity and Mortality

Twenty-four animals completed the study. Three of the animals that failed to complete the study died within 1 week postinfarction and the remaining animal, which was a sham control, died at 7 weeks postinfarction. No dogs developed infections or had insufficient MI.

Recovery of Global Cardiac Performance With Hybrid Therapy

Global cardiac performance after the treatment was assessed serially and comprehensively by MDCT and cardiac catheterization. Both LVEDV and LVESV tended to increase after MI induction in the sham group (Figure 1, *A* and *B*). LVEDV was significantly smaller in the hybrid therapy group compared with the sham group at 3 and 5 weeks postinfarction, and significantly smaller than in both the ONO-1301 alone and sham groups at 8 weeks postinfarction. LVESV in the hybrid therapy group was significantly smaller than that in the sham group at 3 and 5 weeks, and was significantly smaller than that in the other groups at 8 weeks. As a result, LV ejection fraction was significantly greater in the hybrid therapy group compared with the sham group at 3 and 5 weeks, and significantly greater than in the other groups at 8 weeks (Figure 1, *C*).

The LV end-diastolic sphericity index was significantly greater in the hybrid therapy group compared with the ONO-1301 alone and sham groups at 8 weeks postinfarction (Figure 1, *D*). The LV end-systolic sphericity index decreased in all groups at 1 week postinfarction, whereas at 8 weeks the LV end-systolic sphericity index had decreased

ET/BS

TABLE 1. Cardiac catheterization data

	Hybrid therapy	Cardiac support device alone	ONO-1301 alone	Sham
dp/dt maximum (mm Hg/s)				
LV	1822 ± 83*,†,‡	1584 ± 114	1601 ± 91	1238 ± 127
RV	547 ± 101	450 ± 53	539 ± 79	443 ± 86
Ees (mm Hg/mL)				
LV	10 ± 1*,†,‡	7 ± 1	8 ± 1	4 ± 1
RV	3 ± 1	3 ± 1	3 ± 1	2 ± 1
−dp/dt minimum (mm Hg/s)				
LV	1553 ± 61*,†,‡	1303 ± 71	1387 ± 64	1061 ± 107
RV	407 ± 59	378 ± 67	412 ± 88	333 ± 78
Time constant of relaxation (s)				
LV	33 ± 4*,†	42 ± 3	36 ± 3	47 ± 5
RV	39 ± 6	40 ± 2	38 ± 4	46 ± 6

Data are mean ± standard deviation. *RV*, Right ventricular; *LV*, left ventricular. *$P < .05$ versus sham. †$P < .05$ versus cardiac support device alone. ‡$P < .05$ versus ONO-1301 alone.

further in the sham group, remained the same in the cardiac support device alone and ONO-1301 alone groups, and recovered in the hybrid therapy group (Figure 1, *E*).

In addition, systolic function represented by LV dp/dt max and Ees at 8 weeks was greater in the cardiac support device alone and ONO-1301 alone groups compared with the sham group, whereas the hybrid therapy showed significantly greater dp/dt max and Ees than the other groups (Table 1). LV -dp/dt min, which represents diastolic function, also was significantly greater in the hybrid therapy group at 8 weeks than in the other groups. LV time constant of relaxation, which is also an index of diastolic function, was significantly smaller in the hybrid therapy group at 8 weeks postinfarction than in the cardiac support device alone and sham groups. There were no significant differences in any of these parameters in the right ventricle.

MI induction also resulted in an increase in plasma NT-proBNP, assessed by an enzyme-linked immunosorbent assay kit (Cardiopet proBNP; IDEXX Laboratories, Tokyo, Japan), at 1 week postinfarction (Figure 1, *F*). NT-proBNP continued to increase in the sham group, whereas the increase was suppressed in each of the other groups after treatment. NT-proBNP decreased gradually in the hybrid therapy group and was significantly lower than in the sham group at 5 weeks, and was significantly lower than in the other 2 groups at 8 weeks.

Functional Recovery of Infarct Border Area With Hybrid Therapy

Regional LV wall motion was evaluated using speckle-tracking echocardiography to dissect region-specific functional effects of the treatment. The infarct area showed a significant and marked reduction in the radial strain after induction of MI, with no significant differences among the 4 groups (Table 2). Radial strain levels in the border area decreased similarly in all groups at 1 week postinfarction, although at 8 weeks the hybrid therapy group showed the greatest recovery in this area. There was a marked decrease in radial strain in the remote area in the sham group at 8 weeks, but there was little change throughout the study in the other groups.

Reduction in Global End-Systolic/Diastolic Wall Stress With Hybrid Therapy

Changes in global end-systolic/end-diastolic wall stresses after treatment were assessed from MDCT and catheterization data (Table 2). Similar increases in global end-systolic wall stress were observed in all groups at 1 week postinfarction. At 8 weeks postinfarction, however, there was a further increase in the sham group, a slight reduction in the cardiac support device alone group, and almost no change in the ONO-1301 alone group, whereas global end-systolic wall stress was lowest in the hybrid therapy group. Similar increases in global end-diastolic wall stress were observed in all groups at 1 week postinfarction. The sham group showed a marked increase at 8 weeks postinfarction, whereas the hybrid therapy and cardiac support device alone groups showed notable reductions. Global end-diastolic wall stress was significantly lower in the hybrid therapy group compared with the ONO-1301 alone and sham groups at 8 weeks.

ONO-1301 Induced Angiogenic Myocardial Effects in Chronic MI

The angiogenic effects of the treatment were evaluated by assessing global myocardial blood flow at rest by ^{13}N-ammonia PET at 8 weeks postinfarction. Myocardial blood flow in the hybrid therapy group was similar to that in the ONO-1301 group, and both were significantly higher than in the cardiac support device alone and sham groups (Figure 2). Capillary densities in the border and remote areas at 8 weeks postinfarction, which was measured by immunostaining for CD31, was significantly greater in the hybrid therapy group than in the cardiac support device alone and sham groups (Figure 3, *A*).

ET/BS

TABLE 2. Regional left ventricular wall motion and global left ventricular wall stress

	Hybrid therapy	Cardiac support device alone	ONO-1301 alone	Sham
Radial strain in the MI area (%)				
Pre-infarction	21.4 ± 2.3	20.9 ± 1.0	21.7 ± 2.4	22.4 ± 2.3
1 week post-infarction	7.1 ± 1.0	6.7 ± 0.7	7.5 ± 0.9	7.0 ± 1.0
8 weeks postinfarction	8.7 ± 1.2	7.3 ± 0.4	7.5 ± 1.3	6.7 ± 1.0
Radial strain in the border area (%)				
Pre-infarction	22.2 ± 2.6	21.8 ± 2.5	22.0 ± 1.6	21.3 ± 1.8
1 week postinfarction	10.4 ± 1.9	10.3 ± 1.9	11.2 ± 1.5	11.5 ± 1.9
8 weeks postinfarction	14.7 ± 1.1*,†,‡	10.8 ± 0.2	13.1 ± 1.7	8.1 ± 1.1
Radial strain in the remote area (%)				
Pre-infarction	20.7 ± 2.3	21.6 ± 2.0	21.0 ± 2.8	21.2 ± 2.7
1 week postinfarction	19.2 ± 2.1	20.5 ± 1.2	20.9 ± 2.2	19.6 ± 2.0
8 weeks postinfarction	20.2 ± 1.8*	19.7 ± 1.1	20.1 ± 1.5	14.8 ± 1.4
Global end-systolic wall stress (kdyne/cm^2)				
Pre-infarction	79.9 ± 6.8	84 ± 12.0	80.5 ± 8.1	87.6 ± 9.5
1 week postinfarction	108.1 ± 9.1	104.8 ± 11.9	102.7 ± 11.4	107.5 ± 9.6
8 weeks postinfarction	84 ± 5.7*,†,‡	97.7 ± 11.4	104.6 ± 10.0	161.9 ± 9.3
Global end-systolic wall stress (kdyne/cm^2)				
Pre-infarction	13.0 ± 1.5	11.5 ± 1.1	12.0 ± 1.3	12.0 ± 1.6
1 week postinfarction	17.9 ± 1.5	17.1 ± 1.0	17.0 ± 1.4	16.4 ± 2.5
8 weeks postinfarction	14.0 ± 2.5*,‡	14.0 ± 1.8	18.0 ± 1.5	24.4 ± 3.6

Data are mean ± standard deviation. *MI*, Myocardial infarction. *$P < .05$ versus sham. †$P < .05$ versus cardiac support device alone. ‡$P < .05$ versus ONO-1301 alone.

Histologic Evidence of Reversal of LV Remodeling With Hybrid Therapy

Pathologic cardiomyocyte hypertrophy and interstitial fibrosis in the border and remote areas at 8 weeks postinfarction were assessed by periodic acid-Schiff and Masson trichrome staining, respectively, to evaluate the degree of reversal of LV remodeling induced by each treatment (Figure 3, *B* and *C*). Cardiomyocyte diameters were significantly smaller in the border area in the hybrid therapy group compared with the ONO-1301 alone and sham groups, and were significantly smaller in the remote area compared with the sham group. In addition, there was significantly less interstitial fibrosis in the hybrid therapy group compared with the cardiac support device alone, ONO-1301 alone, and sham groups in the border area, and less than in the sham group in the remote area.

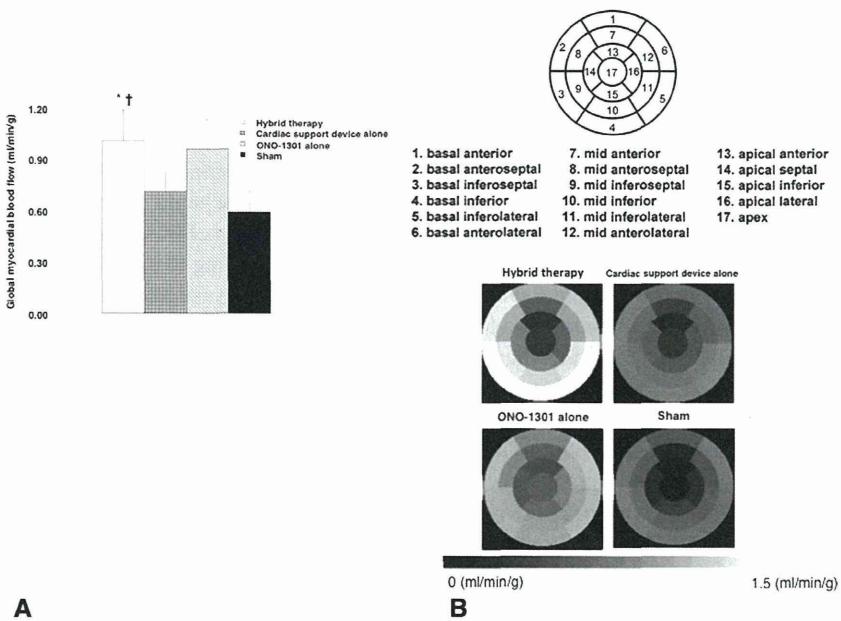

FIGURE 2. A, Global myocardial blood flow assessed by PET at 8 weeks postinfarction. B, Myocardial blood flow divided into 17 segments recommended by the American Heart Association. *$P < .05$ versus sham, †$P < .05$ versus cardiac support device alone.

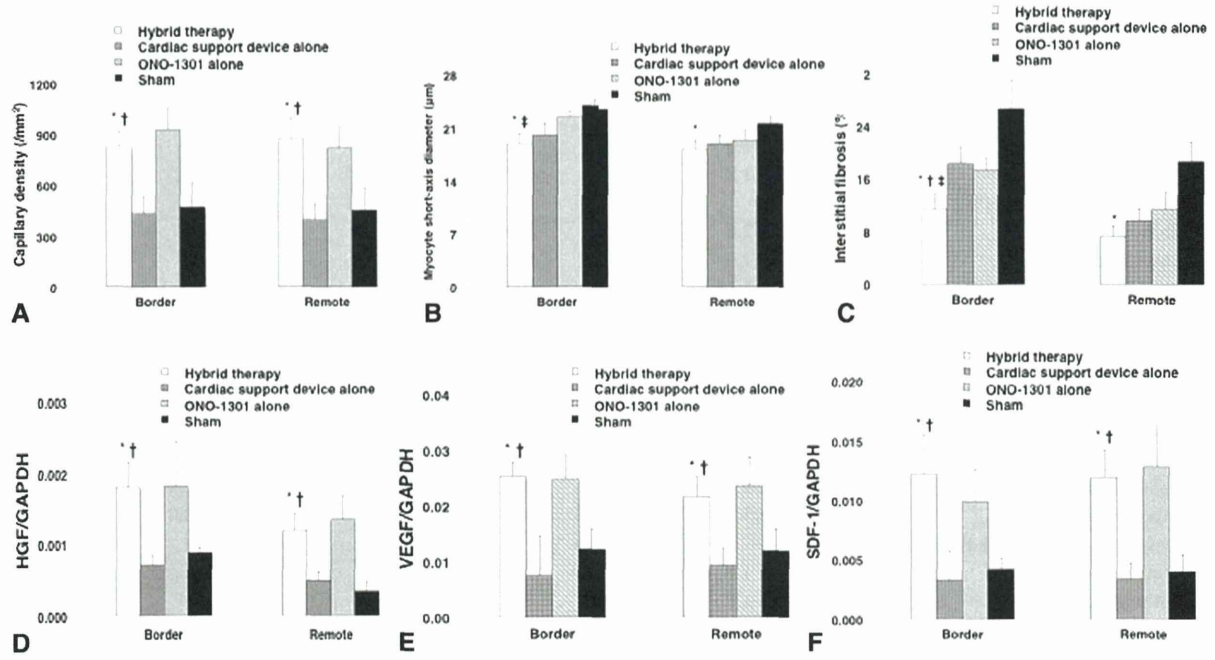

FIGURE 3. Histologic evaluation at 8 weeks postinfarction. A, Capillary density, (B) myocyte short-axis diameter, and (C) interstitial fibrosis in the border and remote areas. Expression levels of (D) HGF, (E) VEGF, and (F) SDF-1 in the border and remote areas quantified by real-time polymerase chain reaction at 8 weeks postinfarction. *$P < .05$ versus sham, †$P < .05$ versus cardiac support device alone. *GAPDH*, Glyceraldehyde 3-phosphate dehydrogenase; *HGF*, hepatocyte growth factor; *VEGF*, vascular endothelial growth factor; *SDF-1*; stromal cell–derived factor-1.

Up-Regulation of Cardiac Protective Factors

Real-time polymerase chain reaction was performed at 8 weeks postinfarction to determine the effects of the treatment on gene expression of major cardiac protective factors, such as HGF, VEGF and SDF-1 (Figure 3, *D-F*). Expression of HGF, VEGF, and SDF-1 in both the border and remote areas were similar in the hybrid therapy and ONO-1301 groups, and significantly higher in these 2 groups than in the cardiac support device alone and sham groups ($P < .05$).

DISCUSSION

This study examined the therapeutic efficacy of hybrid therapy, comprising a cardiac support device and a synthetic prostacyclin agonist (ONO-1301), in a canine model of ischemic cardiomyopathy, compared with the efficacy of either treatment alone. Hybrid therapy significantly improved both systolic and diastolic functions and reduced LV wall stress compared with the other treatments, and histologic examination indicated significantly greater reversal of LV remodeling in the hybrid therapy group. These results were reflected by a significantly greater reduction of NT-proBNP by hybrid therapy.

The cardiac support device used in this study comprised a net made of polyglycolic acid, which is a hydrolytically bioabsorbable polymer. This represents a major difference from the net used in previous studies,[3-5] and was designed to remain around the heart for approximately 10 weeks by adjusting the diameter of the thread. The cardiac support device remained in place at 8 weeks postinfarction, although it had become hydrolyzed to some extent. Our net was functionally equivalent to the nets used in previous studies; it prevented dilatation of the left ventricle, improved the LV sphericity index, and reduced diastolic LV wall stress, thus avoiding the positive feedback loop of cardiac dilatation, the change from an efficient ellipsoidal to a spherical LV chamber, interstitial fibrosis, and, ultimately, heart failure that occurs in ischemic dilated cardiomyopathy.[9] However, one disadvantage of this bioabsorbable net is that it could allow LV remodeling to progress after absorption. The present study did not investigate this aspect and further studies are needed to assess the relative advantages and disadvantages of bioabsorbable and nonabsorbable cardiac support devices.

ONO-1301 is a synthetic prostacyclin agonist that is not yet used in clinical practice. However, several experimental studies have shown its therapeutic efficacy in ischemic and nonischemic cardiomyopathy.[10-12] ONO-1301 was administered to the heart differently in the current study compared with previous studies,[10-12] but its plasma concentrations and reversal of LV remodeling were similar to those seen in previous studies, suggesting that this mode of administration was appropriate. In addition, ONO-1301 administration by incorporation in the cardiac support device could decrease